Sea ice and mixed layer depth influence on nitrate depletion and associated isotopic effects in the Drake Passage – Weddell Sea region, Southern Ocean

Aymeric P. M. Servettaz[1,2,*], Yuta Isaji[1], Chisato Yoshikawa[1], Yanghee Jang[3], Boo-Keun Khim[4,*], Yeongjun Ryu[5], Daniel M. Sigman[5], Nanako O. Ogawa[1], Francisco J. Jiménez-Espejo[1,6], Naohiko Ohkouchi[1]

[1]Biogeochemistry Research Center, Japan Agency for Marine-Earth Science and Technology, Yokosuka, 237-0061 Kanagawa, Japan
[2]Institute of Arctic Climate and Environment Research, Japan Agency for Marine-Earth Science and Technology, Yokosuka, 237-0061 Kanagawa, Japan
[3]Marine Radioactive Monitoring Group, Marine Environment Research Institute, Korea Marine Environment Management Corporation, Busan 49111, Korea
[4]Department of Oceanography and Marine Research Institute, Pusan National University, Busan 46241, Korea
[5]Department of Geosciences, Princeton University, Princeton, New Jersey 08544, United States of America
[6]Instituto Andaluz de Ciencias de la Tierra, Spanish Research Council, 18100 Armilla, Granada, Spain
*Correspondence should be addressed to: A.P.M Servettaz (servettaza@jamstec.go.jp) and B.-K. Khim (bkkhim@pusan.ac.kr)

Abstract. The regions near the Antarctic Peninsula in the Southern Ocean are highly productive, with notable phytoplanktonic blooms in the ice-free season. The primary productivity is sustained by the supply of nutrients from convective mixing with ~~nitrate~~nutrient-rich subsurface waters, which promotes rapid phytoplankton growth as the sea ice melts in spring and summer. Surface waters are marked by the contrast between the warmer Drake Passage and the colder Weddell Sea, and seasonal duration of sea ice cover varies accordingly. Sea ice exerts multiple controls over primary production, by shading the light entering the ocean and stratifying the upper ocean with freshening by ice melt. However, the interaction between sea ice and productivity remains poorly characterized because satellites are unable to quantify biomass in partially ice-covered ocean, and direct measurements are too scarce to characterize the seasonally varying productivity. Here we evaluate productivity by assessing removal of nitrate from surface waters by biological nutrient utilization, and study the associated change in $\delta^{15}N$ of nitrate. We use a combination of bottle samples and *in situ* nitrate measurements from published databases, completed by two transects with isotopic measurements. The timing of sea ice melt date conditions the initiation of nitrate drawdown, but the annual minimum of nitrate only weakly correlates with sea ice concentration. As previously reported, we observe that $\delta^{15}N$ of nitrate increases with nitrate depletion. Interestingly, the lowest nitrate depletion and $\delta^{15}N$ values are found in the central region of N-S transects, where intermediate temperature and sea ice conditions prevail. Deeper mixing in waters that passed through the northern Bransfield Strait may explain higher nitrate concentration due to both a greater nitrate ~~resupply~~concentration at the beginning of the growth season and reduced productivity under light limitation in deeply mixed waters, confirmed by ~~isotopic fractionation effects during nitrate uptake and~~ nitrogen isotope modelling. This highlights the importance of oceanographic controls on productivity patterns in sea-iced regions in the Southern Ocean.

1. Introduction

In the Southern Ocean (SO), phytoplanktonic blooms develop near the Antarctic continent, in the seasonally ice-covered region and in coastal polynyas (Soppa et al., 2016). The marginal ice zone, where sea ice is present but scattered, contributes to a large part of SO productivity (Arrigo et al., 1998; Savidge et al., 1996). Coastal regions around the Antarctic Peninsula are particularly productive as apparent from satellite-based ocean color scanning ~~(Arrigo et al., 2008; Moreau et al., 2020), which stands out from the low-chlorophyll and high-nutrients waters that characterize most of the SO. Oceanic regions south of the Polar Front play an important role in carbon sequestration, due to the high efficiency of carbon export in areas of deepwater formation (DeVries et al., 2012; Gruber et al., 2009; Huang and Fassbender, 2024; Sabine et al., 2004; Wang et al., 2023).~~ (Arrigo et al., 2008; Moreau et al., 2020), which stands out from the low-chlorophyll and high-nutrient waters that characterize most of the SO. The SO is also a major component of oceanic circulation, with upwelling of deep waters contribute to the high nutrient concentration and

47 degassing of carbon into the atmosphere (Marshall and Speer, 2012; Morrison et al., 2015). Understanding
48 productivity patterns and limitations in the seasonally ice-covered SO is thus an important aspect of the global climate.

49 The Antarctic Peninsula and surrounding ~~oceans~~waters constitute one of the fastest warming regions in the Southern
50 Hemisphere (Fan et al., 2014; Jones et al., 2016), and yet challenges remain to understand how primary productivity
51 will react to such warming. Although ~~increase of~~increases in surface water chlorophyll concentration may hint ~~towards~~
52 ~~increased~~at increasing open-water productivity (Moreau et al., 2015), this method does not account for productivity
53 within the marginal ice zone and may primarily reflect the shift from marginal ice zone productivity to open-water
54 productivity due to longer ice-free season. ~~–~~The presence of sea ice prevents the estimation of chlorophyll
55 concentration from satellites, hampering our ability to ~~remotely~~ evaluate the productivity of seasonally ice-covered
56 regions by remote-sensing methods (Bélanger et al., 2007). While *in situ* quantification of chlorophyll concentration
57 may be useful to estimate biomass of primary producers, it only provides information at a given date, and because
58 such measurements are rarely repeated throughout a growth season, they cannot be used to quantify seasonal
59 productivity and export. Indeed, blooming phases in the SO are marked by a high renewal rate of phytoplankton, with
60 turnover rate of phytoplankton reaching 1 day^{-1} (Arteaga et al., 2020). Alternative productivity estimates have been
61 proposed, relying on the quantification of nutrient uptake by primary producers to estimate production and export in
62 the SO ~~(Moreau et al., 2020).~~(Lourey and Trull, 2001; Moreau et al., 2020; Nelson et al., 2002; Pondaven et al., 2000).
63 This quantification relies on the seasonal dynamics of nutrient resupply: deep mixing in winter replenishes the nutrient
64 pool, whereas surface stratification during productive season limits exchanges with underlying water, creating a
65 nutrient budget that will be consumed by primary producers (Codispoti et al., 2013). This method does not account
66 for regenerated nutrients within the surface layer by heterotrophic activity during growth season (Fripiat et al., 2015),
67 but is useful to quantify the seasonal export of organic matter as sinking particles (Flynn et al., 2021; Mdutyana et al.,
68 2020).

69 ~~In the SO, upwelling~~Nitrate is a major source of nitrogen for microorganisms (Ohkouchi and Takano, 2014), with
70 additional variable contributions of ammonium, nitrite, and urea throughout the season (Goeyens et al., 1995;
71 Mengesha et al., 1998). While N_2 fixation can be an alternative nitrogen source in oligotrophic subtropical seas, this
72 contribution is negligible in the SO (Zehr and Capone, 2021). In winter between the ice edge and the Polar Front,
73 nitrification is an important source of regenerated nitrate (Smart et al., 2015), causing the net primary productivity and
74 net nitrogen uptake to be decoupled (Mdutyana et al., 2020). In summer, however, primary productivity is primarily
75 supported by nitrate both in the ice-free SO (Mdutyana et al., 2020) and the seasonally ice-covered zone (DiFiore et
76 al., 2009). In the Weddell Sea (WS), where sea ice concentration (SIC) is usually high, nitrification is slower,
77 suggesting that nitrate utilization may reflect directly net primary productivity (Flynn et al., 2021). Quantifying nitrate
78 depletion in surface water can therefore be used to estimate productivity in summer, or at least organic matter exported
79 to deeper waters. North of the Polar Front in the SO, where there is a strong northward decline in nitrate concentration,
80 there can be significant northward transport of nitrate in surface layer (DiFiore et al., 2006; Sigman et al., 1999).
81 However, this is less of a consideration south of the Polar Front, where horizontal gradients in surface nitrate
82 concentration are typically weak. For the Drake Passage–Weddell Sea region, we aim to evaluate the factors that
83 control nitrate depletion, and thus, net productivity and export.

84 In the SO, several environmental factors can limit phytoplankton growth and primary productivity. Upwelling of
85 nutrient-rich Circumpolar Deep Water at the Antarctic divergence supplies substantial ~~amount of nitrate and phosphate,~~
86 ~~so phytoplanktonic growth may rather be limited by iron and silicate (M. Franck et al., 2000; Moore et al.,~~
87 ~~2002).~~amounts of nitrate and phosphate, so phytoplanktonic growth may rather be limited by light, iron, silicate, or
88 some combination of them (Franck et al., 2000; Moore et al., 2002). In the Drake Passage and offshore west peninsula
89 shelf break, the dissolved iron content is extremely low even at some locations over the continental shelf (< 0.1 nmol
90 kg^{-1}), and thus limits productivity (Annett et al., 2017)… The Antarctic Peninsula side of the Weddell Sea receives
91 iron from melting icebergs, which contributes to dissolved iron concentration slightly higher than the central Weddell
92 Sea or the Drake Passage, especially over the continental shelf where concentrations exceed 0.2 nmol kg^{-1} (Klunder
93 et al., 2014). In the coastal regions around the Antarctic Peninsula and nearby islands, dissolved iron is abundantly
94 supplied by desorption from sediment on the shelves or the coasts, glacier melt, and dust deposition (Ardelan et al.,
95 2010; Jiang et al., 2019; Sherrell et al., 2018). Therefore, contrary to the largest part of the SO, iron is not the limiting
96 factor on phytoplanktonic growth in coastal areas such as in the Bransfield Strait (hereafter abbreviated BS, Frants et

97 al., 2013; Measures et al., 2013). Rather, light availability, controlled by ice shading and vertical mixing, limits
98 phytoplankton growth in ~~these areas~~the BS (Gonçalves-Araujo et al., 2015), which is especially true for winter when
99 light intensity is low (Hatta et al., 2013). This makes it an area of particular interest for studying the relationship
100 between sea ice cover and primary productivity.

101 Sea ice has two opposite effects on light availability: ~~ice~~Ice shades underlying water when it is present, but its melting
102 releases buoyant freshwater that stabilizes the density structure of upper water column and maintains phytoplankton
103 community in euphotic zone (Taylor et al., 2013). We thus hypothesize that sea ice melt contributes to thinning the
104 mixed layer, above which the water is actively mixed by winds. Besides, in areas of sea ice formation, brine rejection
105 ~~favorizes~~favors winter convective mixing and nutrient influx from nitrate-rich subsurface waters. This replenishes
106 surface water nutrients, which may then be used next growing season by primary producers. While some algae also
107 develop within brines and pools of sea ice, their contribution to seasonal biomass productivity is relatively small
108 (Arrigo, 2017). Due to its complexity and opposite effects, the influence of sea ice on seasonally integrated
109 phytoplankton productivity remains poorly characterized.

110 ~~Nitrate is a major source of nitrogen for microorganisms (Ohkouchi and Takano, 2014), with additional variable~~
111 ~~contributions of nitrite, ammonium, and urea throughout the season (Goeyens et al., 1995; Mengesha et al., 1998).~~
112 ~~While N₂ fixation can be an alternative nitrogen source in oligotrophic subtropical seas, this contribution is negligible~~
113 ~~in the SO (Zehr and Capone, 2021). In winter between the ice edge and the Polar Front, nitrification is an important~~
114 ~~source of regenerated nitrate (Smart et al., 2015), causing the net primary productivity and net nitrogen uptake to be~~
115 ~~decoupled (Mdutyana et al., 2020). In summer, however, primary productivity is primarily supported by nitrate both~~
116 ~~in the ice-free SO (Mdutyana et al., 2020) and the seasonally ice-covered zone (DiFiore et al., 2009). In the Weddell~~
117 ~~Sea (WS), where sea ice concentration (SIC) is usually high, nitrification is slower, suggesting that nitrate utilization~~
118 ~~may reflect directly net primary productivity (Flynn et al., 2021). Quantifying nitrate depletion in surface water can~~
119 ~~therefore be used to estimate productivity in summer, or at least organic matter exported to deeper waters.~~

120 In this study, we explore the relationship between nitrate concentration and sea ice characteristics in the SO near the
121 tip of the Antarctic Peninsula, to clarify the impact of sea ice on phytoplankton productivity. We first compare satellite-
122 derived estimations of SIC by area, available year-round, to numerous nutrient concentration that has been widely
123 measured in the SO both with regular sampling ~~(Olsen et al., 2016)~~(Olsen et al., 2016) and automated *in situ*
124 quantification (Johnson et al., 2017). ~~We also describe in further detail a transect of nitrate concentration and its~~
125 ~~nitrogen isotope, which is expected to record isotopic effects during nitrate consumption by primary producers~~
126 ~~(DiFiore et al., 2009; Sigman et al., 1999). The summarized data is then explained with an isotope-enabled ecosystem~~
127 ~~model~~Isotopes can be used to track environmental processes. They are used, for example, in paleoenvironment studies
128 to infer changes that occurred in the past (e.g. using N isotopes: Studer et al., 2015). Knowing how nitrogen isotopes
129 relate to nitrate concentration in the modern ocean opens the use of nitrogen isotopes as a tracer of past nitrate changes.
130 Therefore, we study the link between nitrogen isotopes and nitrate concentration using both observational data and
131 isotope-enabled simulations. To this end, we describe in further detail a previously unpublished transect of the
132 concentration and nitrogen isotopic composition of nitrate, interpreted with the help of model simulations in three
133 oceanic locations.

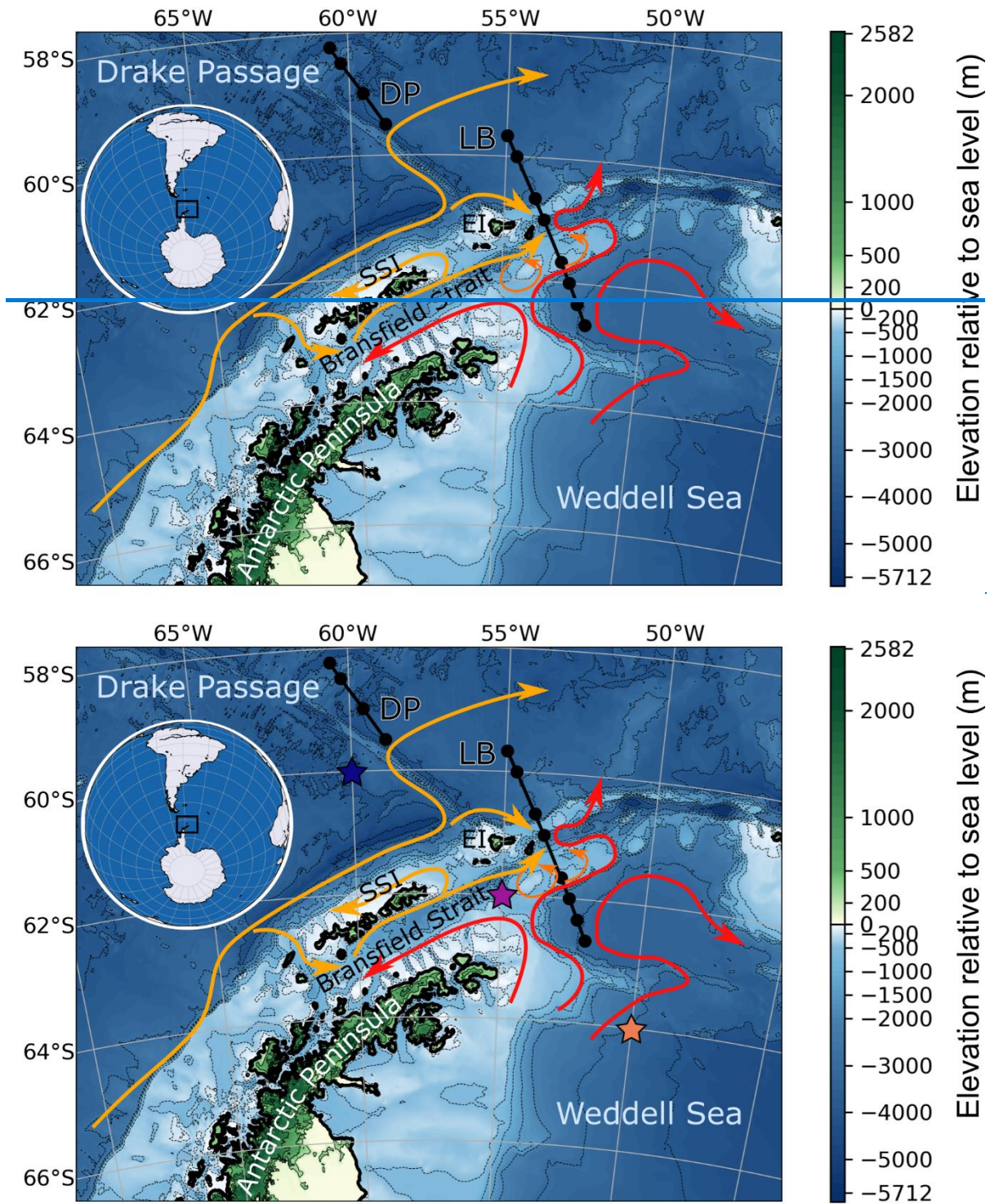134 **2. Oceanographic setting**

Figure 1. Regional map of the northern Antarctic Peninsula, Bransfield Strait, South Shetland Islands (SSI), Elephant Island (EI), and parts of the Weddell Sea and Drake Passage. Arrows highlight the surface water circulation, orange for water originating from the west side, and red for water exiting the Weddell Gyre (Moffat and Meredith, 2018; Thompson et al., 2009). DP and LB refer to two transects discussed in Sect. 4.1; black dots represent the location of bottle sampling stations. Elevation from ETOPO 2022 (NOAA, 2022). Colored stars indicate the location of the three points represented in model simulations (Sect. 4.2.4)

143 While some studies have described the relationship between sea ice and phytoplankton development in other regions
144 of the SO (e.g. von Berg et al., 2020; Briggs et al., 2018; Taylor et al., 2013), we focus here on the region around the
145 northern tip of the Antarctic Peninsula, from DP to WS, with a particular focus on the BS. West Antarctic Peninsula
146 and BS are coastal regions with non-depleted surface iron (Jiang et al., 2019), meaning that phytoplankton growth is
147 more susceptible to be limited by light, as modulated by shading and stratification processes related to ice cover and
148 its melt. Moreover, the West Antarctic Peninsula is the region with the fastest decreasing trend of ice concentration
149 (Jones et al., 2016), raising the question of how productivity will change with decreasing ice cover.

150 North of the Antarctic Peninsula, two surface water masses with distinct properties converge in the BS (Fig. 1; Sangrà
151 et al., 2011). Transitional Zonal Water with Weddell Sea influence (TWW) enters BS from the southeast via the
152 westward coastal current, running along the tip of the Antarctic Peninsula. In the northwest of the BS, Transitional
153 Zonal Water with Bellingshausen influence (TBW) enters via a branching derived from the Antarctic Circumpolar
154 Current, and flows northeastward in the Bransfield Current along the South Shetland Islands (SSI). Further east, this
155 current divides into a return current north of SSI (Moffat and Meredith, 2018) and an eastward branch passing south
156 of Elephant Island (Gordon et al., 2000; Thompson et al., 2009). TBW and TWW are separated by a front with a
157 surface gradient of temperature extending to 50-100 m depth, the Peninsula Front, and subsurface gradient, the
158 Bransfield Front, located further north beneath the Bransfield Current jet at depths of 150 to 500 m (Sangrà et al.,
159 2011). The Bransfield Current is associated with TWB-containing anticyclonic eddies in the upper 80 m at its southern
160 boundary (Thompson et al., 2009). The colder TWW supports the persistence of sea ice for a longer part of the year
161 in the southeast of the Antarctic Peninsula (Fig. 2). Relative contribution of these two surface water masses to BS, and
162 the position of the front separating them, has been suspected to vary with westerly wind intensity (Vorrath et al., 2020).
163 The water masses properties condition the development of primary producers. ~~Previous studies have found higher~~
164 ~~concentration of chlorophyll in the TWB, that was interpreted as warm waters with a shallow pycnocline being more~~
165 ~~productive (Gonçalves-Araujo et al., 2015; La et al., 2019; Pereira Granja Russo et al., 2018)~~Previous studies have
166 found higher concentration of chlorophyll in the TWB, that was interpreted as warm waters with a shallow pycnocline
167 being more productive (Gonçalves-Araujo et al., 2015; La et al., 2019; Russo et al., 2018).
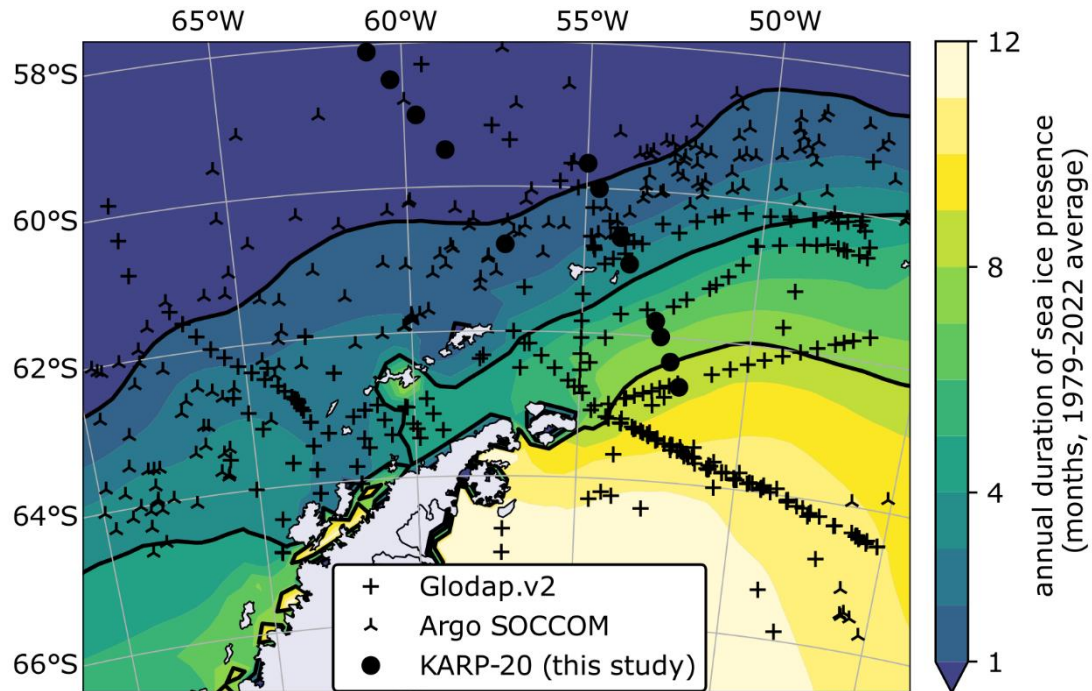
168

169 **Figure 2. Map of sea ice seasonality in the Southern Ocean and nitrate data location. Duration of sea ice presence in months**
170 **per year, defined as the number of months where sea ice concentration is greater than 15% by area (color scale, with black**
171 **contour lines at 1, 4, and 8 months). Sea ice in coastal areas is reportedly inaccurate due to the coarse resolution of the**

sensor (Lavergne 2023). Symbols indicate the location of nitrate concentration data used in this study, classified by data
173 **source.**

3. Material and methods

175 A large number of measurements have been made publicly available in recent years through data repositories. We
176 briefly describe the datasets used, and additional original data presented in this study. We use a regional subsection of
177 the datasets around the Antarctic Peninsula (Fig. 2).

3.1 KARP-20 Nitrate concentrations and isotopes

179 The Korea Antarctic Research Program 20th expedition (KARP-20) conducted Conductivity-Temperature-Depth
180 (CTD) profile using SBE CTD 911plus along three transects in the DP region between the 1st and the 31st of December
181 2006. Water bottle samples were collected for nitrate analysis at 13 stations (black circles on Fig. 2) with 12 water
182 depth sampled at each location. Salinity and temperature from CTD were used to determine the potential density
183 anomaly, σ_0.

184 Nitrate concentration of each bottle was determined after reduction of nitrate and nitrite to nitric oxide using a V(III)
185 reagent, then quantified by chemiluminescence (Braman and Hendrix, 1989). Our concentration measurements
186 include nitrite, whose contribution is expected to be small in the SO in summer (Thomas et al., 2024). In addition to
187 nitrate concentration, the δ^{15}N of ~~nitrates were~~nitrate was analyzed using the "denitrifier method", where nitrate is
188 converted to nitrous oxide gas by ~~modified~~a strain of denitrifying bacteria lacking nitrous oxide reductase activity
189 (Sigman et al., 2001). ~~After transformation of nitrate to nitrous oxide, the nitrogen isotopic composition of resulting~~
190 ~~nitrous oxide is analyzed with gas chromatography isotope ratio mass spectrometry (GC IRMS) at Princeton~~
191 ~~University (USA).~~After transformation of nitrate to nitrous oxide, the nitrogen isotopic composition of resulting
192 nitrous oxide is analyzed with a custom-built in-line preparation and purification system connected to a gas-source
193 isotope ratio mass spectrometer (Thermo Fisher MAT253) at Princeton University (USA) (Weigand et al., 2016).

194 The denitrifier method analyzes the δ^{15}N of both nitrate and nitrite. Nitrite can have substantially lower δ^{15}N due to
195 nitrate-nitrite equilibrium isotope effect (Kemeny et al., 2016). Given this interconversion between nitrate and nitrite
196 N, the isotopic effect of nitrate assimilation affects the δ^{15}N of both nitrate and nitrite, hence it is more accurate to
197 consider the δ^{15}N of the sum of nitrate and nitrite when evaluating the assimilation isotope effect (Fripiat et al., 2019).
198 Acidified water samples might have lost most of their nitrite due to volatility of nitric acid, which would bias the δ^{15}N
199 values towards the δ^{15}N of nitrate (Fripiat et al., 2019). However, the KARP-20 samples were not acidified prior to
200 isotopic analysis and thus likely retained both nitrate and nitrite.

3.2 Glodapv2 nitrate concentrations

202 The Global Ocean Data Analysis Project Version 2 (GLODAPv2; ~~Olsen et al., 2016)~~Olsen et al., 2016) is a collection
203 of biogeochemical bottle data, extending from the World Ocean Circulation Experiment database with quality-
204 controlled additions from more recent cruises. A thorough description of the GLODAPv2.2022 used here is given by
205 Lauvset et al. (2022). Nitrate concentrations in bottle samples are typically determined using the colorimetric
206 absorbance measurement after reduction to nitrite (Armstrong et al., 1967). Measurements included in GLODAPv2
207 database were quality checked and outliers are removed from the published dataset (Key et al., 2015). Here we only
208 briefly describe how we selected samples used in our study. We defined a regional subset around the Antarctic
209 Peninsula with 45 °W–78 °W and 56 °S–66 °S boundaries, and selected stations where sea ice was present in the year
210 prior to sampling, thus excluding the permanently open ocean zone (see Sect. 3.5 for sea ice data used). Bottles
211 included in this subset were collected between September 1989 and January 2016. In addition to the nitrate value, we
212 use the potential density anomaly (σ_0) for definition of mixed layer depth (MLD). In the subregion defined for the
213 present study, a total of 187 stations with at least one nitrate measurement above MLD were used (the calculation of
214 MLD used here is given in Section 3.4). While nitrate concentration measurements are very precise with around 0.2%
215 uncertainty, comparison of deep bottles (>1000 m) with nearby (<250 km) measurements give variations usually lower
216 than 2% of the measured value (Aoyama, 2020), which can provide a base estimate of consistency of repeat nitrate

217 measurements, and adjustment were made in GLODAPv2 which resulted in a similar consistency level (Lauvset et
218 al., 2022), even if it is not uncertainty in the strict sense.

3.3 SOCCOM Argo floats *in situ* nitrate estimation

220 Recent developments of ultraviolet spectrophotometers nitrate sensors provide *in situ* quantification of nitrate
221 concentrations using its absorbance in the ultraviolet band, without requiring chemical transformation (Johnson et al.,
222 2013; Johnson and Coletti, 2002; MacIntyre et al., 2009). When mounted on profiling floats, they can profile the
223 nitrate content of the water column, and are set to measure 300 profiles at a rate of one profile every ~5 days which
224 can make the battery last for a couple of years (Johnson et al., 2013). The SO Carbon and Climate Observations and
225 Modeling (SOCCOM) has deployed 295 floats in the SO, equipped with biogeochemistry sensors including
226 submersible nitrate sensor (as of May 2024. source:
227 https://www3.mbari.org/soccom/tables/SOCCOM_float_performance.html). A description and evaluation of
228 accuracy of nitrate sensors used on SOCCOM floats is given in ~~Wanninkhof et al. (2016)~~Wanninkhof et al. (2016).
229 We use a quality-controlled dataset where nitrate sensors were calibrated prior to deployment, and offset and drift
230 were adjusted throughout the float service time using known concentration at depths below 1000 m as a reference for
231 calibration ~~(Maurer et al., 2021)~~(Maurer et al., 2021). This lowers the uncertainty on nitrate concentrations to 0.5
232 μmol kg^{-1}. SOCCOM floats have previously been used to assess nitrate drawdown and net community production
233 (Johnson et al., 2017), and hereafter we specifically assess the influence of sea ice on nitrate drawdown. We use a
234 total of 194 profiles from 16 floats, all measured in the regional subset previously defined, dated between January
235 2016 and June 2022.

3.4 Definition of mixed layer depth and surface nitrate depletion

237 The surface mixed layer depicts a layer actively mixed by wind activity, leading to homogenous physical and chemical
238 properties. Its depth is controlled by the strength of winds and the density gradients, such as a change of temperature
239 or an increase of density indicates the MLD. In the SO, it is preferable to use a density criterion due to the low
240 temperatures throughout the year and significant contribution of meltwater to salinity changes. Therefore, we define
241 the MLD as the depth with a density increased by $\Delta\sigma = 0.03$ kg m^{-3} relative to the reference density taken at 10-m
242 depth (de Boyer Montégut et al., 2004).

243 Surface nitrate concentrations presented in this study are an average of all available measurement points in the mixed
244 layer~~.~~ (Fig. 3 shows summer nitrate concentrations). For summer samples, we also use nitrate depletion, defined as
245 the difference in nitrate concentration between the surface mixed layer and a subsurface water referred to as Winter
246 Water (WW; ~~Goeyens et al., 1995).~~Moreau et al., 2020; Spira et al., 2024). WW describes water that was last mixed
247 during the previous winter, when cold surface temperature leads to higher density, thereby increasing the depth of
248 mixing. Similarly to Flynn et al. (2021), we define the WW layer as the layer between the MLD and the depth of the
249 temperature minimum within 20 to 200 m below the MLD. WW serves as a reference for ocean conditions before the
250 seasonal growth of phytoplankton, therefore nitrate depletion is defined as the difference between nitrate concentration
251 in the WW (average of all measurements in the depth range) minus surface nitrate concentration.

252 Input of meltwater from sea ice with low nitrate concentration could bias this depletion value due to the dilution of
253 nitrate in surface waters. We corrected for this dilution effect following the method of Flynn et al. (2021), proposed
254 for the WS. To evaluate the maximum dilution potential, we also use the minimal value for nitrate concentration in
255 sea ice of 1 μmol kg^{-1} reported for the Bellingshausen and Weddell Seas (Fripiat et al., 2014). Note that, as in the
256 original study by Flynn et al. (2021), this correction only marginally affects the depletion values; in the samples
257 considered here, the average summer salinity decrease is 0.18 PSU (1st decile – 9th decile range: 0.04–0.36 PSU), and
258 result in an average dilution correction of 0.18 μMol kg^{-1} (1st decile – 9th decile range: 0.04–0.37 μmol kg^{-1}) for nitrate
259 depletions. The slightly greater dilution effect for strong salinity decrease is due to the higher seawater nitrate
260 concentration with high sea ice meltwater contribution. ~~Therefore,~~The amplitude of the ~~interpretations that we would~~
261 ~~make in~~dilution effect is too small to impact the conclusions of this article ~~do not differ~~. We hereafter refer to
262 meltwater-dilution corrected nitrate depletion as "nitrate depletion (corrected)".

3.5 Sea ice concentration

264 We use daily SIC retrieved from version 3 of the EUMETSAT Ocean and Sea Ice Satellite Application Facility sea-
265 ice products for the 1979-2022 period (OSI SAF 2022a, 2022b; updated from Lavergne et al., 2019). This 25 km
266 resolution reconstruction is based on microwave emissivity of surface ocean, with SIC calculated from brightness
267 temperature. Accuracy of SIC by area was evaluated to 8 % in version 2 of this dataset (Lavergne et al. 2019). Updated
268 processing chain and auxiliary climate fields in version 3 used here result in a reduced bias (Lavergne et al., 2023).

269 For each nitrate concentration measurement, we extracted the SIC on the grid cell corresponding to measurement
270 location, at daily resolution on the year preceding the measurement date. We therefore retrieve the sea ice condition
271 in the time leading up to nitrate measurement. This approach enables monitoring the anomalies in SIC on the year of
272 measurement, since sea ice conditions at the measurement location may substantially differ from average due to the
273 high ~~international~~interannual variability (Parkinson and Cavalieri, 2012; Wang and Wu, 2021).

3.6 Nitrogen isotope modelling

275 We simulated the nitrogen cycle in the surface ocean using an isotope enabled ecosystem model. This model has six
276 compartments, phytoplankton (PHY), zooplankton (ZOO), particulate organic nitrogen (PON), dissolved organic
277 nitrogen (DON), nitrate (NO_3^-), and ammonium (NH_4^+). The prognostic variables are the N and ^{15}N concentrations.
278 The equations and parameters excluding nitrification are the same as those used by Yoshikawa et al., (2005), which
279 successfully simulated nitrogen isotope observations in the Sea of Okhotsk, a high-latitude marginal sea. The
280 equations and parameters for nitrification are the same as those used by Yoshikawa et al. (2022), which includes
281 photoinhibition terms. The nitrogen isotope fractionation parameters are the same as those used by ~~Yoshikawa et al.~~
282 ~~(2024)~~Yoshikawa et al. (2024).

283 We applied the model to the ocean environment in three locations around the Antarctic Peninsula: Drake Passage (DP:
284 60 °S, 60 °W), Eastern Bransfield Strait (BS: 62 °S, 55 °W) and Weddell Sea (WS: 64 °S, 50 °W). This model has
285 two vertical layers (surface layer: 0-20 m; subsurface layer: 20-120 m). Light intensity at the surface was taken from
286 long term mean daily net shortwave radiation fluxes of NCEP-NCAR Reanalysis (Kalnay et al., 1996). ~~Water~~
287 ~~temperature at upper and lower layers and MLD were taken from the World Ocean Atlas 2018 (Garcia et al., 2019).~~
288 ~~Water exchange between the surface and subsurface layers, and between the subsurface layer and the layer deeper~~
289 ~~than 120 m are changed seasonally in conjunction with the MLD. Boundary conditions at 120 m depth for the nitrate~~
290 ~~concentration were taken from the World Ocean Atlas 2018 (Garcia et al., 2019) and its δ^{15}N value was fixed to 5‰~~
291 ~~which is in the range of the observations at 120 m during KARP-20 (Sect.~~Water temperature at upper and lower layers
292 and MLD were taken from the World Ocean Atlas 2018 (Garcia et al., 2019). Water exchange between the surface
293 and subsurface layers, and between the subsurface layer and the layer deeper than 120 m, are changed seasonally in
294 conjunction with the MLD. Boundary conditions at 120 m depth for the nitrate concentration were taken from the
295 World Ocean Atlas 2018 (Garcia et al., 2019) and its δ^{15}N value was fixed to 5‰, which is in the range of the
296 observations at 120 m during KARP-20 (Sect. 4.2). The model was integrated for a 4-year spin-up period, and then
297 used to simulate a period of 1 year.

4. Results and Discussion

4.1 Sea ice impact on nitrate depletion

300 In this section we assess the impact of sea ice on nitrate depletion, to verify the hypothesis that large seasonal variations
301 in sea ice could contribute to stratification of the surface water~~, as sea~~. Sea ice retreat~~-~~ enhances light availability and
302 nutrient consumption by primary producers (Sallée et al., 2010) while reducing the available nutrient pool due to the
303 thinning of the surface mixed layer (Smith, and Nelson, 1986; Taylor et al., 2013).

304 We use the sea ice seasonality at the location where the nitrate concentration was measured. We did not backtrack
305 either the water parcel or the sea ice~~. Also, we assume~~, assuming that ~~sea ice~~the seasonality of ice at the point of ~~nitrate~~
306 measurement ~~is similar to~~(fixed location) resembles that of the water parcel ~~present at the time of nitrate sampling, *i.e.*~~
307 ~~not resolving the effects of ocean circulation or drifted ice over the course of a season.~~in which nitrate was measured
308 (moving parcel). A parcel-tracking approach would be technically possible using coupled ocean-sea ice model, but
309 we do not expect significant improvement of our results due to limitations in modelled ice drift (Uotila et al., 2014).
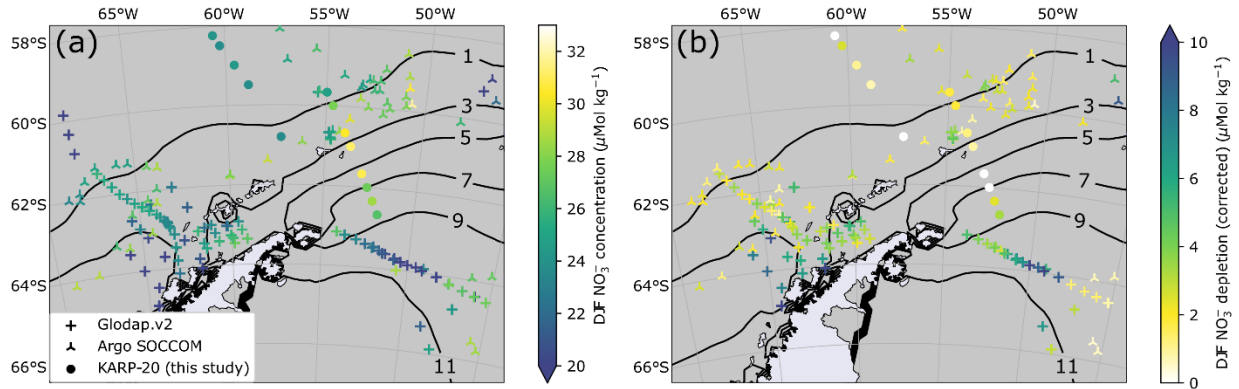
4.1.1 Spatial patterns

311

Figure 3. (a) Map of summer surface water nitrate concentration (color scale) classified by data source (symbol type). Contour lines indicate the 1979-2022 average sea ice presence duration in months per year. (b) same as (a), but for summer nitrate depletion (corrected). The definition of summer depletion and its correction are given in Sect. 3.4. The lower number of points for nitrate depletion results from the absence of nitrate concentration data in the subsurface layer of winter water.

Spatial patterns of summer (December, January, and February: DJF) nitrate concentration (Fig. 3a) and depletion (Fig. 3b) do not particularly match the sea ice presence gradient (Fig. 2). Nitrate depletion is intense in the western BS and Gerlache Strait, with values consistently exceeding 5 µmol kg^{-1}, ~~as described by~~ which was attributed to thriving phytoplankton blooms in the very stable surface waters (Castro et al. ~~(~~2002~~) which first described this data included in Glodap.v2. They attributed this strong depletion to thriving phytoplankton blooms in the very stable surface waters.~~). In addition, strong depletion values close to 10 µmol kg^{-1} are observed in the WS around 50 °W, contrasting with lower depletion values further east, of profiles on the same cruise (Fahrbach, 1993). KARP-20 nitrate concentrations east of Elephant Island (61 °S, 54 °W to 62 °S, 52 °W) are among the highest nitrate concentrations measured for summertime, with values exceeding 30 µmol kg^{-1}. KARP-20 stations also reveal that nitrate is not depleted relative to subsurface waters in the outlet of the BS (discussed in further detail in Sect. 4.1). Generally, nitrate concentration or depletion do not correspond spatially to sea ice duration (Fig. ~~2~~ 3).

4.1.2 Timing of ice melt

The biological activity in the SO is restricted in the austral spring by light, both from low incident light angle and from the shading effect of remaining sea ice. Near the Antarctic Peninsula, the duration of sea ice cover varies latitudinally from the quasi-permanently ice-covered WS to the open ocean in the center of DP (Fig. 2). As the sea ice retreats, the light limitation is expected to be reduced, and the water column is stabilized by release of low-density meltwater (Taylor et al., 2013). This would favor phytoplanktonic growth and nitrate consumption.

To visualize the effect of ice retreat on nutrient drawdown, we show how nitrate depletion (surface minus subsurface concentration, see Sect. 3.4) varies during the season, and relative to the day of ice melt at different locations around the Antarctic Peninsula (Fig. 4). In September and October, the surface nitrate depletion is minimal, owing to deep mixing and limited nitrate utilization. In late spring to early summer (November-December), the surface nitrate is more depleted, although approximately half of the waters sampled during these months have nitrate depletion of less than 3 µmol kg^{-1}. In January and February, the surface nitrate is depleted by more than 5 µmol kg^{-1} at most sampling stations. Nitrate depletion exceeding 5 µmol kg^{-1} is encountered throughout the summer. In March, the deepening of MLD vertically homogenizes the nitrate concentrations, and in conjunction with the slowing of biological uptake in autumn, the nitrate depletion in surface water decreases.

Timing of ice melt controls the initiation of phytoplankton bloom and associated nutrient uptake through the formation of buoyant surface meltwater (Fig. 4). Although few samples were recovered prior to complete ice melt, the nitrate concentrations measured before ice melt are marginally depleted relative to subsurface waters, with less than 5 µmol kg^{-1} difference. The highest of these pre-ice melt depletions comes from the profiles measured in July when the

346 water column may not have been homogenized, and the depletion is probably a remnant of the previous year. Low
347 nitrate depletions prior to ice melt results from the low biological activity, the larger nutrient resupply due to ~~non-~~
348 ~~segregated~~well-mixed surface waters, or a combination of both. After sea ice melts, depletion greater than 5 μmol kg^{-1}
349 is frequent, but ~~not observed in all samples. More~~more than half of nitrate depletion values are still lower than 5
350 μmol kg^{-1}. Although there is a large spread of nitrate depletion values at any time after the ice melt, the highest
351 depletions are reached after about ~~50~~70 days, which may reflect the entire duration of the phytoplankton bloom
352 following ice melt, with the lowest nutrient values after the bloom phase ends (Arteaga et al., 2020, and supplement
353 therein). During early summer, productivity evolves from regenerated to new production and the nitrate uptake
354 increases as any ammonium remaining from the winter is consumed first (Savoye et al., 2004). Later in the season,
355 phytoplankton growth slows down (Arteaga et al., 2020), and the relative contribution of regenerated nutrients to
356 biological production increases (decrease in the f-ratio, ~~Fripiat et al., 2015; Mdutyana et al., 2020).~~Fripiat et al., 2015;
357 Mdutyana et al., 2020; Sambrotto and Mace, 2000). Additionally, weakening of the stratification in later season can
358 lead to decrease in surface nitrate depletion, as mixed layer gradually deepens and incorporates nitrate-rich water from
359 the subsurface. Melting of sea ice can also favor phytoplankton bloom by releasing iron that concentrates in sea ice
360 (Boyd and Ellwood, 2010; Lannuzel et al., 2016), in particular for regions where iron is limiting such as the DP.

361 In summary, nitrate depletion is ~~strongest when the sea ice melting precedes light maximum by~~generally greatest
362 about ~~50~~70 days after ice has melted (Fig. ~~4a~~4b). It points out the high nutrient utilization in well-lit buoyant lens of
363 meltwater, supporting the hypothesis of sea ice control on nutrient utilization. However, the large variability of nitrate
364 depletion noted at any point in time indicates that while nutrient utilization may be optimal at a certain timing after
365 ice melts, nutrient depletion will not necessarily occur at this time. Three-season monitoring near Palmer Station
366 suggests that stratification by surface temperature increase after sea ice has melted is the main condition for bloom
367 initiation (Moline and Prézelin, 1996), which can explain the equivocal relationship between sea ice retreat and bloom
368 initiation: temperature remains low as long as sea ice remains, but sea ice melt is not necessarily immediately followed
369 by a temperature increase. Temperature rise may trigger the bloom initiation at a delay with ice melt by enhancing
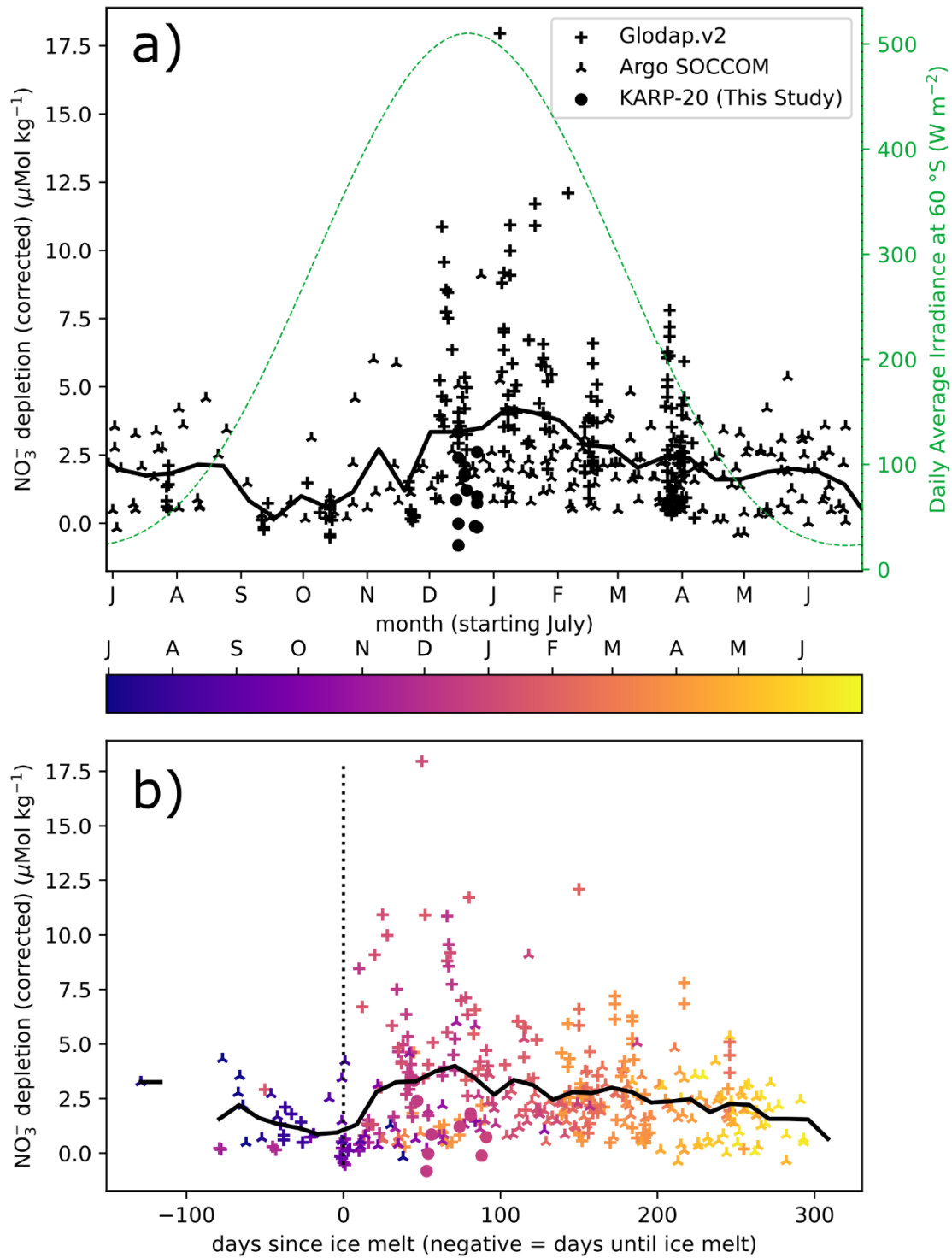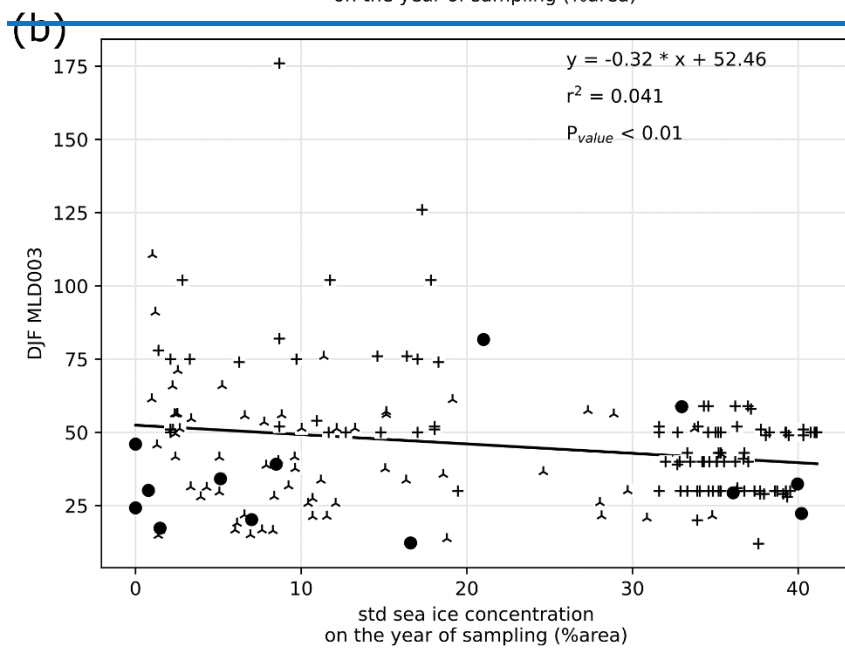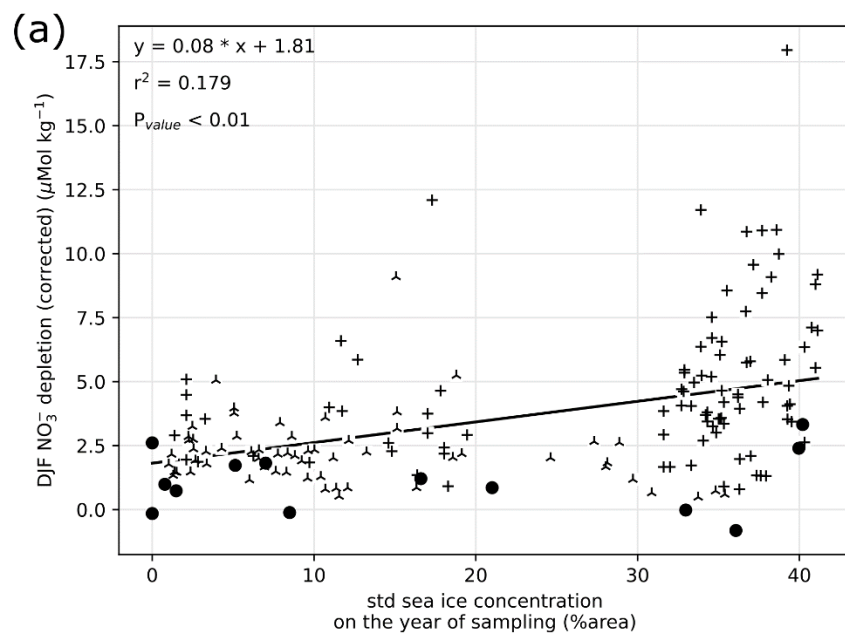370 both stratification and productivity.
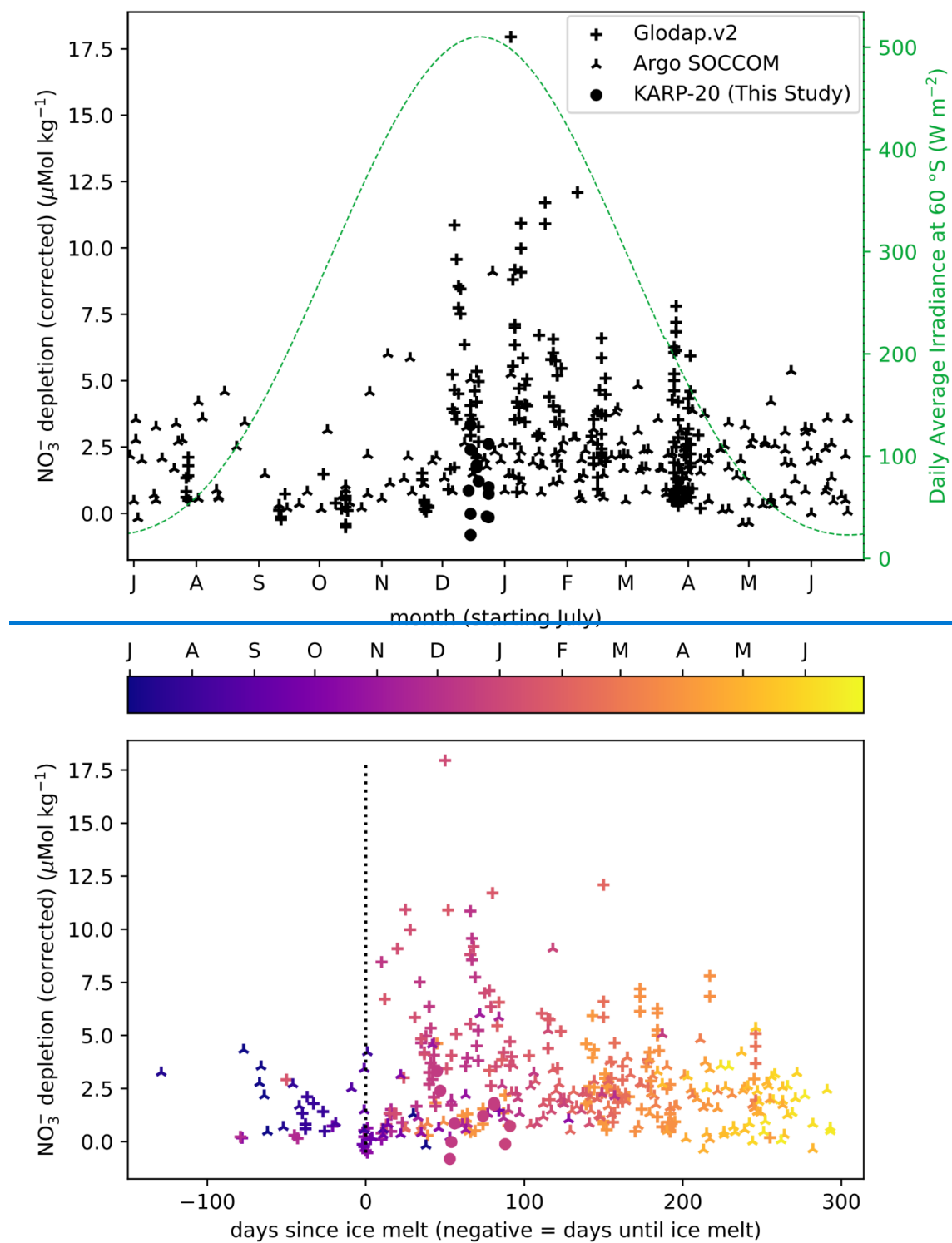
Figure 4. Nitrate depletion as a function of day of year (a) and day since ice melt (b)~~.~~), defined as the number of days spent with ice concentration below 15%. The annual cycle of insolation is given as daily average irradiance at the top of atmosphere at 60 °S (green dashed line). The color of points in (b) indicates the timing in the year. The 25-day rolling average is represented by tick black continuous line on both plots.
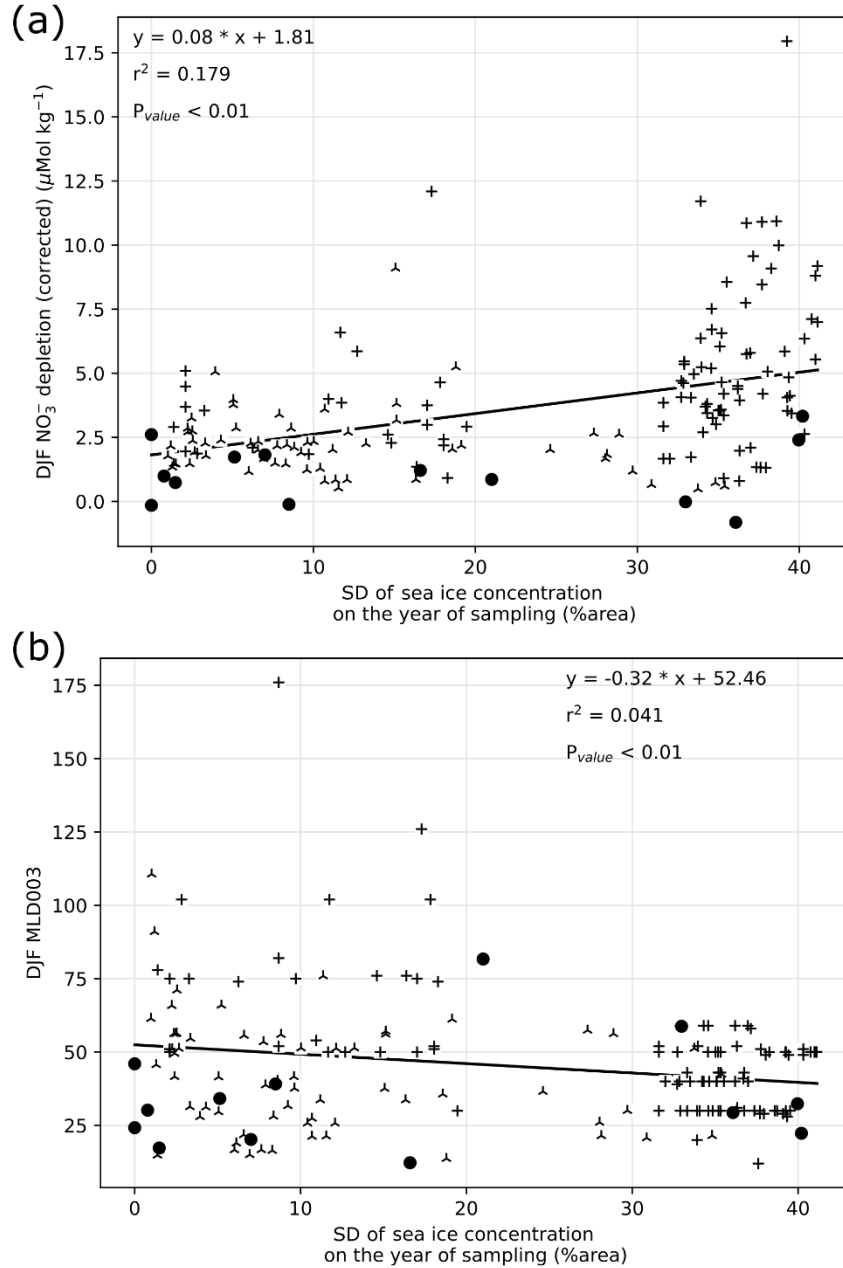
4.1.3 Seasonal range of ice concentration

(a)

y = 0.08 * x + 1.81

r^2 = 0.179

P_{value} < 0.01

DJF NO$_3^-$ depletion (corrected) (μMol kg^{-1})

std sea ice concentration
on the year of sampling (%area)

(b)

y = -0.32 * x + 52.46

r^2 = 0.041

P_{value} < 0.01

DJF MLD003

std sea ice concentration
on the year of sampling (%area)

378

13

(a)

$y = 0.08 * x + 1.81$

$r^2 = 0.179$

$P_{value} < 0.01$

DJF NO$_3^-$ depletion (corrected) (μMol kg^{-1})

SD of sea ice concentration
on the year of sampling (%area)

(b)

$y = -0.32 * x + 52.46$

$r^2 = 0.041$

$P_{value} < 0.01$

DJF MLD003

SD of sea ice concentration
on the year of sampling (%area)

Figure 5. (a) Summer (December, January, and February: DJF) nitrate depletion as a function of sea ice seasonal range estimated with yearly standard deviation of sea ice concentration. (b) summer (DJF) mixed layer depth (MLD) as a function of sea ice seasonal range. Data source is indicated by symbols, consistently with previous figures.

In this section we investigate whether an increased seasonal variation of the SIC (area coveredcalculated as standard deviation of annual sea ice at daily resolution) would favor nitrate depletion, through the shoaling of the MLD which improves the light availability while reducing the amount of nutrients. (Fig. 5). Although volume or mass of sea ice would be more suited for this comparison, parameters relying on thickness are poorly constrained in the SO (Kwok and Kacimi, 2018; Williams et al., 2015). We thus rely on satellite data to estimate the area of sea ice coverage. We use standard deviation of SIC (SD$_{sic}$) over the year leading up to the sampling to evaluate the range of seasonal changes in sea ice cover. It is preferred over average sea ice to rule out high sea ice cover grid points such as in the WS, where SIC is high year-round, leading to high average and low variability sea ice cover.

14

Summer nitrate depletion varies widely at the regional scale studied here, with values ranging from 0 up to 12.5 μmol kg^{-1}. While most nitrate depletion greater than 5 μmol kg^{-1} occurs at SD_{sic} higher than 10%, there is nevertheless a wide range of nitrate depletion encountered at any SD_{SIC} (Fig. 5a). Notably, non-depleted (depletion < 1 μmol kg^{-1}) waters are observed regardless of the SIC. A weak positive correlation ($r^2 = 0.179$, $p_{value} < 0.01$) between nitrate depletion and SD_{SIC} suggests that about 18 % of the variability of both sea ice and nitrate depletion is shared. Although we cannot conclude on a causal relationship, changes in SIC may at most be responsible for 18% of the variability in nitrate depletion. This low correlation indicates that seasonal amplitude of sea ice alone cannot explain all the variability found in the surface nitrate depletion in summer in this region.

We also tested if high ~~yearly SIC~~SD_{sic} leads to reduced MLD, through the meltwater supply to the surface (sample locations are mostly ice-free in summer, except for a few locations with partial ice cover). Because we analyze the sea ice seasonality at a fixed location for simplicity, this relies on the assumption that sea ice melts locally, ignoring possible ice drift and/or meltwater horizontal transport. Comparing summer MLD with yearly SIC (Fig. 5b) reveals that while stations with yearly SIC exceeding 20 % have a MLD consistently shallower than 60 m, a wide range of MLD is encountered at stations with low SIC, implying control of MLD by additional factors. Indeed, sea ice melting controls freshwater inputs and salinity, but temperature is also an important factor of stability in the sea ice covered section of the SO (Pellichero et al., 2017). Consequently, despite being significantly correlated ($p_{value} < 0.01$), MLD and SIC only share 5.7 % variability ($r^2 = 0.057$). At the regional scale, sea ice seasonality has a limited influence on MLD. In turn, the summer nitrate depletion is mostly independent of sea ice cover, although it is less frequently depleted in waters with scarce sea ice cover.

Reasons to why sea ice seasonality does not control nitrate depletion at the regional scale likely emerge from the variety of settings across fronts and basins around the Antarctic Peninsula. Light limitation is often indirectly linked to sea ice: the removal of shading is not sufficient to trigger bloom and nutrient drawdown (Fig. 4). It is possible that light limitation is relieved with stratification of the upper ocean layer, which can occur with a delay after ice melts~~.~~ ~~Density~~, with temperature-driven stratification. Indeed, density profile and MLD are more likely to be controlled by temperature rather than salinity in the seawaters north of the Peninsula Front (Gonçalves-Araujo et al., 2015), where low inputs of freshwater are compensated by stronger temperature-driven stratification. On the contrary in the WS and southern half of BS, sea ice provides freshwater lowering salinity, but it also buffers the temperature and maintains a cool surface even in the summer. Possible iron supply from ice melt may also increase productivity without changing MLD (Lannuzel et al., 2016), and may partly explain why nitrate depletion is better correlated to SD_{SIC} than MLD. Regional differences in productivity response to MLD were also found West of the AP (Vernet et al., 2008), and chlorophyll *a* concentration in the BS do not appear to correlate with MLD either (Romanova et al., 2021). Given the spatial variability within the study region, it may be hard to infer the general influence of sea ice on productivity for other regions of the SO, which have different limitations. A regional comparison of sea ice extent and chlorophyll a suggests that temperature and nutricline are important drivers in spatial discrepancies (Behera et al., 2020).

4.2 ~~Observation~~Observations and modelling of ^{15}N enrichment

While nitrate concentration does not appear clearly linked to sea ice, investigating the isotopic signature in nitrate may reveal further constraints on nitrate uptake. Additionally, how the nitrogen isotopes relate to nitrate concentration and other environmental processes is necessary information to be able to use isotopes as a tracer of these processes. In this section, we focus on the DP and BS transects (location given in Fig. 1), with measurements of nitrate concentration and δ^{15}N. We verify that the relationship between nitrate concentration and isotopes follows a Rayleigh distillation in this region (Sect. 4.2.2). We then validate our interpretations against an isotope-enabled nitrogen cycle model forced by environmental parameters taken from three characteristic sub-regions (Sect. 4.2.3).

4.2.1 KARP-20 nitrate concentration and δ^{15}N transects

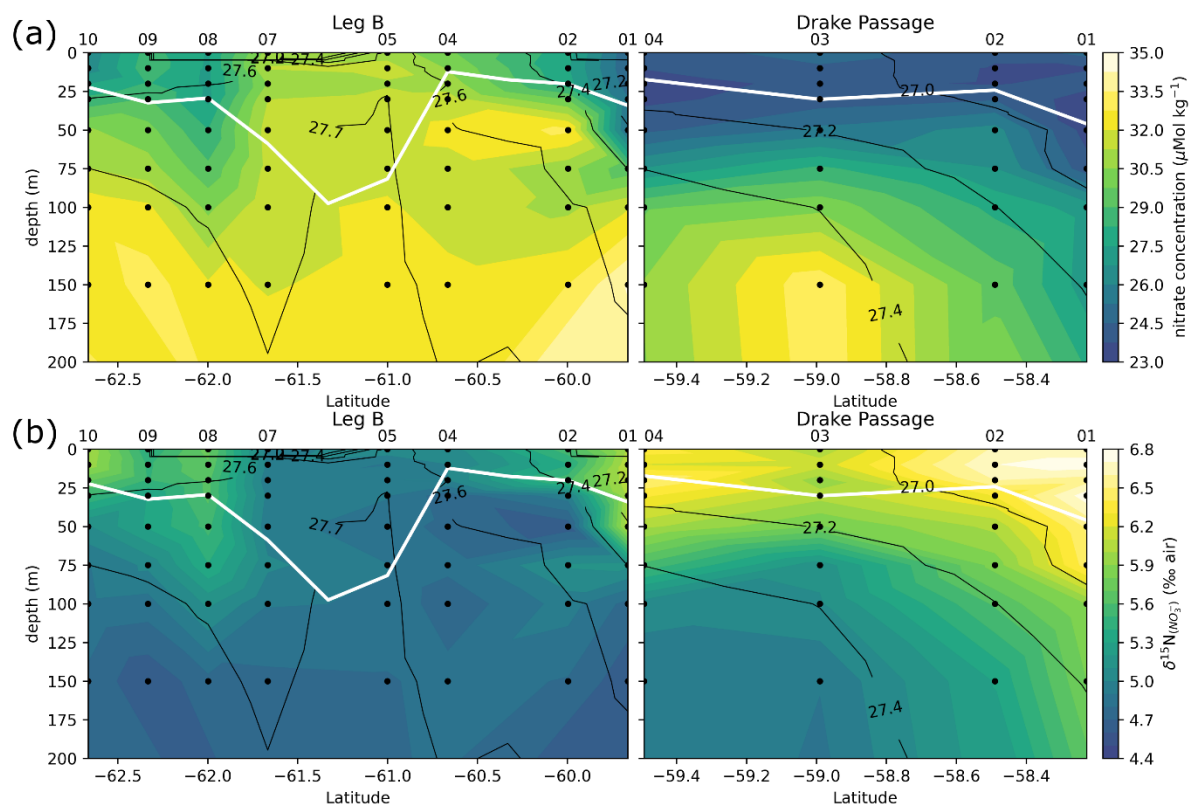**Figure 6. Leg B and Drake Passage Transects, with color shadings of nitrate concentration (a) and δ15N of nitrate (b). Black contours represent the CTD potential density anomaly (σ0 in kg m-3). White line highlights the MLD, computed as the depth with a potential density increased by 0.03 kg m-3 relative to the density at 10 m depth.**
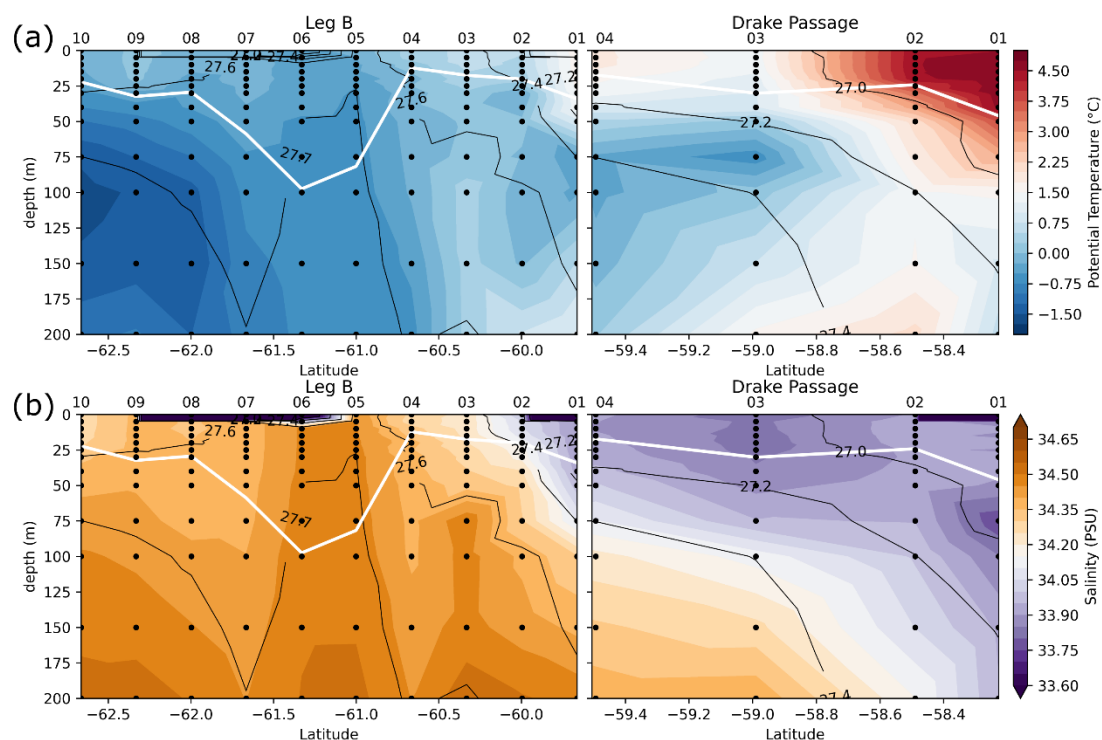

Figure 7. Same as Fig. 6, but for potential temperature (a) and salinity (b).

440 Transects of nitrate concentration in the DP and eastern BS (Fig. 6a) depict the typical SO summer pattern, with partial
441 depletion in the surface waters, down to a minimum of 23 µmol kg^{-1} in the DP, compared to subsurface waters in
442 which concentrations exceed 31 µmol kg^{-1} (profiles also given in Appendix Fig. A1). Isopycnals follow the general
443 SO pattern, with deepening at lower latitudes. An exception is the center section of LB transect (60.7 °S to 61.7 °S),
444 where there is a shoaling of the 27.7 kg m^{-3} isopycnal, indicating the presence of high-density water at relatively
445 shallow depth. The high density is due to higher salinity (>34.45 PSU) of this water rather than temperature (Fig. 7).
446 This center section also has the highest surface nitrate concentration, about 30 µmol kg^{-1}, and the deepest MLD due
447 to the vertically homogenous density. In the DP, surface nitrate concentration is generally lower, and the nitrate
448 concentration appears low even beneath the MLD (Fig. 6).

449 The center section of LB transect with high surface nitrate concentration and deep mixing is in the prolongation of
450 northern BS current that circulated around the SSI and Elephant Islands (Fig. 1). Although its high salinity could
451 correspond to Weddell Sea Water transported along the slope on the western side of the Powell Basin, its intermediate
452 temperature rather supports a western origin (TWB). Physical ocean modelling supported by tidal stations suggests
453 that tidal interaction on the shelf of the SSI arc actively mixes the water, mixing in high salinity from deeper water
454 and homogenizing the density profile (Zhou et al., 2020). The vertical homogeneity of density remains when the water
455 is transported downstream, allowing for the wind mixing to take over and maintain a deep mixed layer, visible in the
456 60.7–61.7 °S section of the LB transect. Activation energy for wind-mixing is lowered in case of lower density
457 gradient (Pollard et al., 1973), which means that a similar wind stress will result in a deeper mixing. Surface nitrate
458 concentration appears closely related to these oceanographic conditions.

459 Two mechanisms may explain higher nitrate concentration in deeply mixed water: (1) quantitatively greater initial
460 nitrate pool, due to a larger volume (or greater resupply) meaning that for an equal uptake per area unit, the
461 concentration remains higher; and (2) lower nitrate uptake due to a limited productivity. Nitrogen isotopes can provide
462 insight into the relationship between nitrate supply and consumption rates, both of which are seasonally changing.

4.2.2 ^{15}N enrichment during Rayleigh distillation

464 Nitrate uptake by phytoplankton is associated with an increase of δ^{15}N of the nitrate remaining in seawater (following
465 the δ notation relative to the ratio ^{15}N/^{14}N in atmospheric N$_2$), due to the preferential uptake of ^{14}N by the
466 microorganisms (Sigman et al., 1999). ~~The uptaken~~Consequently, nitrate concentrations are inversely correlated with
467 δ^{15}N of nitrate in the nutrient-rich SO (Lourey et al., 2003).The consumed nitrate is transformed into organic molecules
468 with an average biosynthetic nitrogen isotope effect ε of around 5‰ (Altabet and Francois, 2001; Sigman et al., 1999;
469 Waser et al., 1998), given by the difference in kinetics of reaction rates between ^{14}N and ^{15}N: $\varepsilon = {}^{14}k/{}^{15}k - 1$.
470 ~~Applied in a Rayleigh distillation, isotope effect can be approximated by~~

471 A system where a component is progressively removed without coincident resupply can be described by the Rayleigh
472 distillation model. It can be applied to describe isotopic fractionation during nitrate uptake in the condition that there
473 is net removal from the water through one process (nitrate assimilation), and the removed nitrate has an isotopic
474 composition that differs from that in the water. In this case, the isotope effect can be quantified by the following
475 approximation using measurable parameters:

476 $$\varepsilon = \frac{\delta^{15}N_{initial} - \delta^{15}N}{\ln(NO_3^-) - \ln(NO_{3\ initial}^-)} \tag{1}$$

477 ~~(Mariotti et al., 1981; Sigman et al., 1999; ε is defined as positive if δ^{15}N of remaining nitrate increases when nitrate~~
478 ~~concentration decreases).~~

479 ~~This effect may be slightly more positive in light-limited environments (DiFiore et al., 2010; Needoba et al., 2004;~~
480 ~~Needoba and Harrison, 2004). Consequently, nitrate concentrations are inversely correlated with δ^{15}N of nitrate in the~~
481 ~~nutrient-rich SO (Lourey et al., 2003; Sigman et al., 1999). In this section, we focus on the KARP 20 transect, with~~
482 ~~measurements of nitrate concentration and δ^{15}N, to gain further insights on nitrate uptake. We then evaluate observed~~
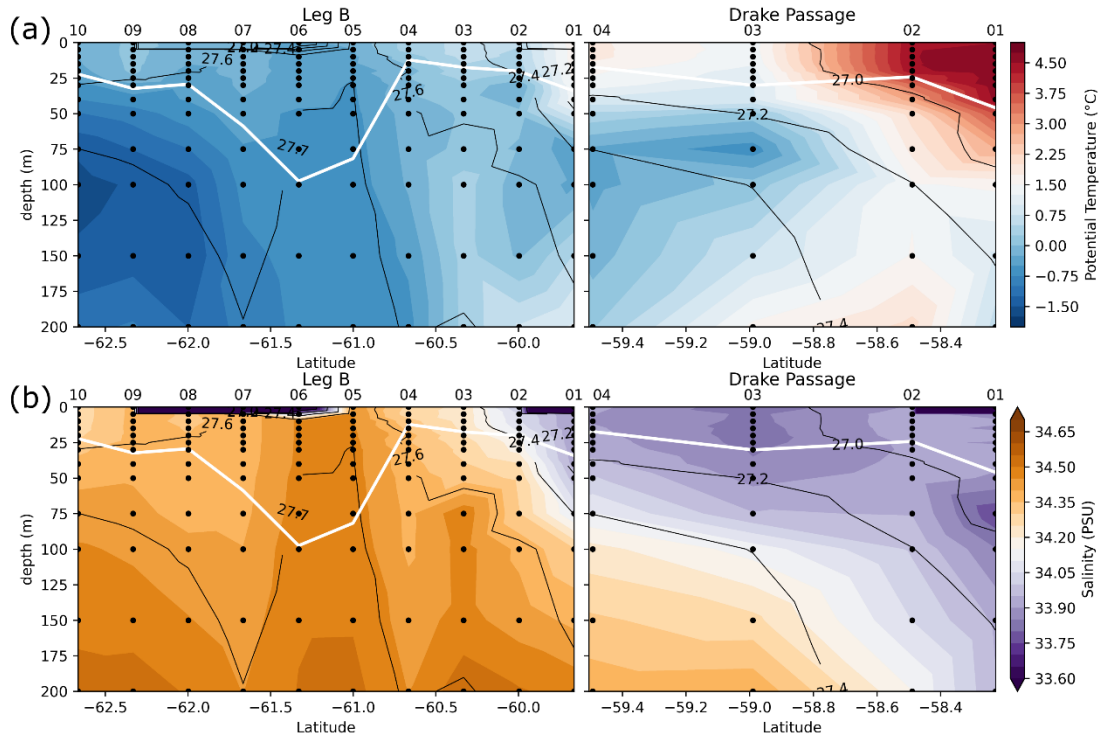483 ~~trends using a nitrogen cycle isotope model with environmental forcings.~~

489

Figure 7. Same as Fig. 6, but for potential temperature (a) and salinity (b).

Transects of nitrate concentration in the DP and eastern BS (Fig. 6a) depict typical SO summer pattern with partial depletion in the surface waters, down to a minimum of 23 μmol kg^{-1} in the DP compared to subsurface waters, where concentrations exceed 31 μmol kg^{-1} (profiles also given in Appendix Fig. A1). Isopycnals follow the general SO pattern with deepening at lower latitudes, except for the center section of LB transect (60.7 °S to 61.7 °S) with a shoaling of the 27.7 kg m^{-3} isopycnal, indicating the presence of high density water at relatively shallow depth. The high density is due to higher salinity (>34.45 PSU) of this water rather than temperature (Fig. 7). This center section also has the highest surface nitrate concentration at about 30 μmol kg^{-1} and the deepest MLD supported by the vertically homogenous density. In the DP, surface nitrate concentration is generally lower, and the nitrate concentration appears low even beneath the MLD (Fig. 6).

The center section of LB transect with high surface nitrate concentration and deep mixing is in the prolongation of northern BS current that circulated around the SSI and Elephant Islands (Fig. 1). Although its high salinity could correspond to Weddell Sea Water transported along the slope on the western side of the Powell Basin, its intermediate temperature rather supports a western origin (TWB). Physical ocean modelling supported by tidal stations suggests that tidal interaction on the shelf of the SSI are actively mixes the water, mixing in high salinity from deeper water and homogenizing the density profile (Zhou et al., 2020). The vertical homogeneity of density remains when the water is transported downstream, allowing for the wind mixing to take over and maintain a deep mixed layer, visible in the 60.7–61.7 °S section of the LB transect. Activation energy for wind-mixing is lowered in case of lower density gradient (Pollard et al., 1973), which means that a similar wind stress will result in a deeper mixing. Surface nitrate concentration appears closely related to oceanographic circulation.

Two mechanisms may explain higher nitrate concentration in deeply mixed water: (1) quantitatively greater initial nitrate pool, due to a larger volume (or greater resupply) meaning that for an equal uptake per area unit, the concentration remains higher; and (2) lower nitrate uptake due to a limited productivity. Nitrogen isotopes can provide insight onto the latter hypothesis.

$$\varepsilon = \frac{\delta^{15}N_{initial} - \delta^{15}N}{\ln(NO_3^-) - \ln(NO_{3\ initial}^-)} \quad (1)$$

519 (Mariotti et al., 1981; Sigman et al., 1999). The isotope effect ε is defined as positive if $\delta^{15}N$ of remaining nitrate
520 increases when nitrate concentration decreases. The initial concentration and isotopic composition refer to that of the
521 nitrate in the water at the beginning of the growth season, which in our case is assumed to be retained in the Winter
522 Water layer (defined in Sect. 3.4).

523 Generally, the $\delta^{15}N$ of nitrate negatively correlates with its ~~concentrations~~concentration: there is a visible
524 correspondence between low surface nitrate ~~concentrations~~concentration (Fig. 6a) and high $\delta^{15}N$ of ~~nitrates~~nitrate (Fig.
525 6b). $\delta^{15}N$ is low (4.5 to 5 ‰) in waters deeper than 125 m, where nitrate concentration exceeds 30 $\mu mol\ kg^{-1}$, and
526 reaches high values of up to 6.8 ‰ near the surface in DP where nitrate concentrations are the lowest ~~(23 μmol kg⁻¹)~~
527 ~~of these transects. This negative correlation is consistent with previous works, and reflects the isotopic fractionation~~
528 ~~during partial uptake of the available nitrate (Altabet, 2006; Lourey et al., 2003; Sigman et al., 1999)~~of these transects
529 (23 $\mu mol\ kg^{-1}$). This negative correlation is consistent with previous work, and reflects the isotopic fractionation
530 during partial uptake of the available nitrate (Altabet, 2006; Fripiat et al., 2019; Lourey et al., 2003; Sigman et al.,
531 1999). While the nitrate reservoir is not strictly isolated in summer, exchanges between surface mixed layer and
532 subsurface waters are limited due to the density gradient preventing wind-activated mixing (Lewis et al., 1986; Pollard
533 et al., 1973). When approximating surface waters above the MLD as a closed system, fractionation during nitrate
534 uptake follows a Rayleigh-type isotopic distillation ~~(Lourey et al., 2003)~~(Lourey et al., 2003). In the Rayleigh
535 distillation, the $\delta^{15}N$ is linearly correlated with the logarithm of nitrate concentration ~~(DiFiore et al., 2009; Mariotti et~~
536 ~~al., 1981)~~(DiFiore et al., 2009; Mariotti et al., 1981). ~~We thus quantify the isotopic effect of nitrate uptake following~~
537 ~~the linear regression on logarithmic concentration scale method (DiFiore et al., 2009; Appendix Fig. A2).~~Given the
538 high correlations at each station between $\delta^{15}N$ and the logarithm of nitrate concentration (Pearson $r^2 > 0.9$ for all
539 stations except LB07 with $r^2 = 0.633$; Fig. A2), the approximation with Rayleigh distillation seems appropriate for
540 the transects presented here.

541

542 The Rayleigh distillation model may not be applicable if changes to the isotopic composition are issued from processes
543 other than nitrate assimilation. Nitrogen recycling through heterotrophic activity may modify the isotopic repartition
544 between organic and dissolved inorganic nitrogen (Sigman and Fripiat, 2019). Recycling of N through nitrification
545 preferentially converts ^{14}N back to nitrate and may decrease the apparent ε of N uptake (DiFiore et al., 2009). In the
546 summer, however, nitrate supplied by nitrification accounts for less than 10 % of nitrate uptake (DiFiore et al., 2010;
547 Flynn et al., 2021; Mdutyana et al., 2020). The nitrogen isotope effect ε in KARP-20 profiles (Fig. 8) is close to
548 previously reported values for ε, so they are in line with low nitrate recycling and the approximate validity of Rayleigh
549 distillation. Light inhibition may underly this lack of nitrification in summer (Mdutyana et al., 2020).
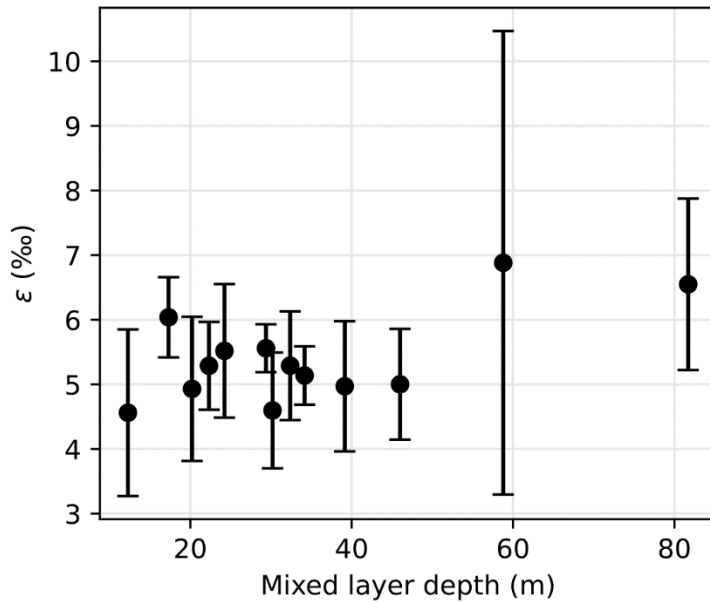
Figure 8. Nitrogen isotope effect ε as a function of the mixed layer depth. Error bars indicate the 95 % confidence interval for ε estimation.

Nitrate assimilation has been reported to imprint a nitrogen isotope effect of about 5 ‰ in SO field studies (DiFiore et al., 2009, 2010; Sigman et al., 1999). Under light limitation, the isotope effect shows notable increase, with values exceeding 8 ‰ (DiFiore et al., 2010), which is considered to be the result of continuous active pumping of nitrate to offset nitrate loss by diffusion through cell membrane, when assimilatory nitrate reduction is slowed by light limited cellular activity (Needoba et al., 2004; Needoba and Harrison, 2004). Here, most profiles support nitrogen isotope effects ε of 5 ‰, as long as the MLD is shallower than 50 m (Fig. 8). The two profiles where the MLD is deeper, which are in the central section of LB at 61 °S and 61.7 °S, indicate slightly higher ε of 6.5 ± 1.4 ‰ and 6.9 ± 3.5 ‰, respectively. These higher ε mark light limitation in deeply mixed surface layers (DiFiore et al., 2010), and therefore support the hypothesis of lower nitrate utilization as a cause for the elevated nitrate concentration in the central section of LB. However, these ε values are lower than those previously reported for comparable MLD in the open Antarctic Zone, where sea ice is typically absent (DiFiore et al., 2010). This is likely due to stronger seasonal variability in the MLD related to the presence of seasonal sea ice in our study, suggesting that the MLD may have been shallower at the start of growth season. The data from DiFiore et al. (2010) for ocean zones with sea ice do not support ε values exceeding 5 ‰, because summer mixed layers in the Indian sector of SO are generally shallower than 50 m. This is consistent with our findings except for the two profiles with deep mixing.

Nitrogen recycling through heterotrophic activity may modify the isotopic repartition between organic and dissolved inorganic nitrogen (Sigman and Fripiat, 2019). Recycling of N through nitrification preferentially converts ^{14}N and may decrease the apparent ε of N uptake (DiFiore et al., 2009). In the summer, however, contribution of regenerated nitrogen to phytoplankton productivity is low, with f ratio usually higher than 0.6 in the BS (Bode et al., 2002) and WS (Flynn et al., 2021), and nitrate supplied by nitrification accounts for less than 10 % of nitrate uptake (Flynn et al., 2021; Mdutyana et al., 2020). This means that more than half of summer nitrogen consumption consists of new nitrate uptake from the environment. Low regeneration rate is due to reduced heterotrophic activity in cold oceans, while light inhibits nitrification in summer. The nitrogen isotope effect ε in KARP 20 profiles is close to or higher than the reported values for ε, so they are in line with low nitrate recycling, not detectible in the nitrogen isotopes.

Despite minor changes in ε in light-limiting conditions, the relationship between nitrate depletion and δ^{15}N elevation that has been previously described in other regions of the SO (DiFiore et al., 2010; Lourey et al., 2003; Sigman et al., 1999) holds true in the ice-covered region of the Antarctic Peninsula.

4.2Nitrate assimilation has been reported to imprint a nitrogen isotope effect of about 5 ‰ in the SO (DiFiore et al., 2009, 2010; Fripiat et al., 2019; Sigman et al., 1999). Some studies have attributed greater isotope effect to continuous active pumping of nitrate to offset nitrate loss by diffusion through cell membrane, when assimilatory nitrate reduction is slowed by light-limited cellular activity (Needoba et al., 2004; Needoba and Harrison, 2004). In the SO, light limitation was proposed as a cause of higher isotopic effects in waters with deeper mixed layers, with values exceeding 8 ‰ (DiFiore et al., 2010), but that finding must be reassessed given the recently recognized role for nitrate-nitrite N isotope exchange in SO waters (Fripiat et al., 2019; Kemeny et al., 2016), which can lead to overestimation of ε if the samples have lost nitrite (e.g., in the case of sample preservation by acidification). Here, we quantify the isotopic effect of nitrate uptake following the linear regression on logarithmic concentration scale method (DiFiore et al., 2009; Appendix Fig. A2), station by station to evaluate spatial changes in fractionation effect during assimilation of nitrate by phytoplankton. Consistent with Fripiat et al. (2019), we find nitrogen isotope effects ε around 5 ‰, insensitive to MLD for MLD ≤ 50 m (Fig. 8). It is possible that still deeper MLDs are associated with higher ε, but the weakness of the regressions make this uncertain (Fig. 8). In any case, lower surface nitrate $\delta^{15}N$ and higher surface nitrate concentrations around 61 °S in the LB transect are in line with environmental limitation of nitrate assimilation, that we attribute to light limitation as MLD is larger at this location.

In summary, our data support that the relationship between nitrate depletion and $\delta^{15}N$ elevation, previously described in other regions of the SO (DiFiore et al., 2010; Lourey et al., 2003; Sigman et al., 1999), holds true in the ice-covered region of the Antarctic Peninsula. The consistency of the data with the Rayleigh model implies that nitrate resupply did not occur late in the summer season, as this would have violated the Rayleigh model and largely removed the surface nitrate $\delta^{15}N$ elevation.

4.2.3 Nitrogen isotope modelling

In this final section, we reproduce the $\delta^{15}N$ signatures of nitrate usinguse a nitrogen isotope box-model (Yoshikawa et al., 2005) in to reproduce the observed differences between three oceanic locations around the Antarctic Peninsula: the seasonally ice covered part of DP (60°S, 60°W), semi-enclosed eastern BS (62°S, 55°W), and the northwestern WS (64°S, 50°W) where sea ice exits the Weddell Gyre.basins of the studied region, which have different sea ice cover duration, and compare them with KARP-20 nitrate patterns. Modelling the nitrogen cycle allows understanding of the seasonal evolution of nitrate concentrations, whereas observations are usually made in a short time frame.

 The model simulates a nitrogen cycle in a sea ice covered ocean, focusing on surface (0-20 m) and subsurface (20-120 m) layers, from inputs of seawater temperature, mixing depth, insolation, and nitrate concentration and its $\delta^{15}N$ at the 120 m boundary condition (Fig. 9). The model has a daily time resolution with a simulation length of one year (after 4 years spin-up), and reproduces an ideal annual cycle at equilibrium, *i.e.* repeating itself given the same forcings. We run three simulations in oceanic locations representative of distinct basins, each with specific ice cover: the seasonally ice-covered part of DP (60°S, 60°W), semi-enclosed eastern BS (62°S, 55°W), and the northwestern WS (64°S, 50°W) where sea ice exits the Weddell Gyre.
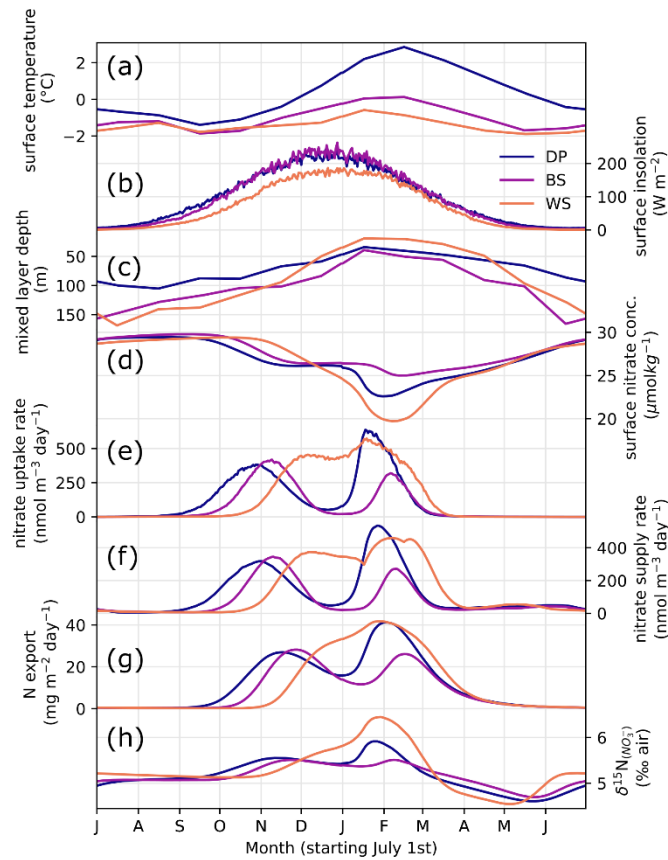
614

Figure 9. Seasonal variability of model forcings and results: surface water temperature (a), insolation (b), MLD (c), surface nitrate concentration (d), nitrate uptake rate in surface model box (e), nitrate supply rate from subsurface to surface (f), sinking particulate N export (g), and δ^{15}N of nitrate in the surface model box (h) in three oceanic locations (DP, BS, and WS).

We first give a brief description of environmental parameters used to constrain the model. Temperature variability is strongest in the DP location (60 °S, 60 °W), which averages 1.7 °C in summer, when BS reaches a maximum of around 0°C (Fig. 9a, Fig. 10a). The temperature at the WS location is buffered by the presence of sea ice, and remains below -0.5°C year-round. Insolation is roughly similar for the three sites, although slightly lower in the WS due to the higher latitude. MLD follows the typical seasonal variability (Behera et al., 2020), shoaling in the spring and summer and deepening during autumn and winter. It is implemented indirectly in the model, regulating the exchange rates between surface and subsurface layers, rather than modifying the layer thickness in the model. The amplitude of MLD variability is greater for BS and WS, where more sea ice is present (Fig. 9c, Fig. 10d). The MLD in BS remains deeper even in summer, averaging 59 m. BS location has an intermediate temperature and yearly sea ice (Fig. 10a, 10b), but also the greatest sea ice standard deviation (Fig. 10c), used to approximate the seasonal variability of sea ice cover here. Despite greater change in sea ice cover, the summer MLD is still greater in BS location, which goes against the hypothesis of a sea ice meltwater induced summer stratification (Taylor et al., 2013), and confirms that sea ice seasonal variability is not the main control on summer MLD in this region (as discussed in Sect. 4.1).

~~The model simulates the N cycle in the surface ocean and its impact on δ^{15}N (Fig. 9d–h, Fig. 10e–k). For DP and BS locations, the resulting annual cycle of seawater nitrate has two peaks of nitrate uptake, corresponding to spring and summer phytoplankton blooms. This matches the two peak chlorophyll seasonality reported for the Antarctic Circumpolar Current (Prend et al., 2022). Consequently, nitrate depletion in the surface waters increases in two steps in spring and summer, with lower minimal concentration at DP location. Although dual blooming is observed in the environment, it usually is not as clear as the idealized cycle produced by the model, with observed maxima overlapping, or double blooms not repeating every year.~~ At the WS location, growth season is shorter due to its onset delayed by

23

639 the late melting of sea ice, resulting in a single yearly maximum rate of nitrate uptake. Nevertheless, WS has a greater
640 nitrate depletion (Fig. 10j) in the surface layer compared to the two other locations, driven by higher nutrient uptake
641 in the strongly stratified surface ocean (Fig. 10f). The BS location with the deepest mixed layer is characterized by a
642 lower nitrate uptake especially in the later part of summer (Fig. 9e), resulting in a lower depletion and higher
643 concentration relative to the two other locations. $\delta^{15}N$ of nitrate (Fig. 10i) scales with the net nitrate uptake (Fig. 10f-
644 h), with maximum ^{15}N-enrichment at WS location, and minimum at BS location. ~~The model~~This matches observations
645 of higher nitrate concentrations in summer north of the Antarctic Peninsula, and around 61 °S in the LB transect. The
646 model also predicts that N export due to sinking particulate organic matter follows the same pattern (Fig. 10k).

647
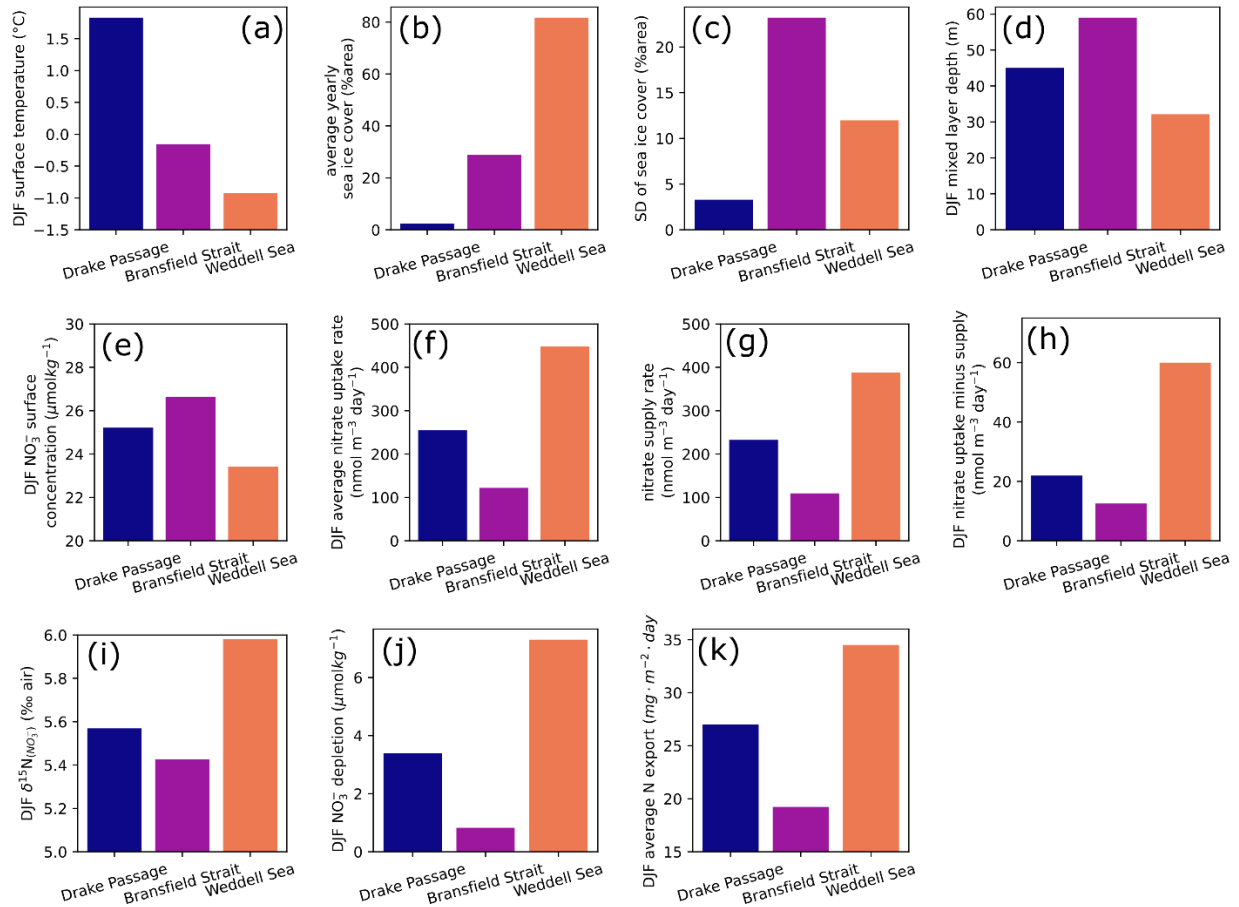
Figure 10. Summer (December, January, and February) averages of model forcings and results for (a) surface water
temperature, (d) mixed layer depth, (e) surface nitrate concentration, (f) nitrate uptake rate by primary producers, (g)
nitrate supply rate from subsurface to surface model layer, (h) difference between uptake and supply rates, (i) $\delta^{15}N$ of
nitrate in surface water, (j) nitrate depletion in the surface water, (k) total nitrogen export in the sinking flux in three
oceanic locations. Yearly sea ice parameters are given for (b) average and (c) standard deviation, used here to quantify
seasonal variability. Upper row plots (a-d) are environmental forcings, with temperature (a) and mixing depth (d) forcing
the model. Lower rows (e-k) describe nitrogen cycle model results.

655 Both in the model results and in the latitudinal transect (Sect. 4.~~1~~2), it appears that the eastern BS has the lowest
656 productivity due to its deeper mixed layer, despite intermediate temperature and sea ice seasonality. The higher surface
657 nitrate concentration of the model for BS matches the 61–62 °S section with high surface nitrate concentration (Fig.
658 6), although absolute values are slightly lower in the model. Timing-wise, the model tends to predict ~~a larger~~
659 ~~divergence of~~that surface nitrate concentration at ~~the~~ BS ~~location in~~is most different from other locations during the
660 later part of summer (around February, Fig. 9), but ~~the~~ December observations of nitrate concentration are already
661 ~~differs in December observations, in part due to a light-limited productivity.~~marked by strong latitudinal differences

662 (Fig. 6a). The area of low nitrate uptake east of the SSI matches the low chlorophyll area in the climatology of surface
663 ocean color (La et al., 2019). The location of BS point chosen for the model may not be exactly in this low chlorophyll
664 area but closer to the Peninsula Front. However, model results should not differ because the two are characterized
665 ~~with~~by a relatively deep summer mixing and similar ice cover. In addition, the eastern BS is notably characterized
666 ~~with~~by a deepening of isopycnals (Frey et al., 2022; Huneke et al., 2016) and deeper chlorophyll maximum ~~(Pereira~~
667 ~~Granja Russo et al., 2018), attesting that the MLD increases eastward, and primary producers are likely dragged~~(Russo
668 et al., 2018), attesting that the MLD increases eastward, and primary producers are likely mixed to deeper waters.

669 In the SO, despite low temperature, a significant portion of particulate organic matter is remineralized in the water
670 column, and nitrogen loss in surface water by sinking particles is compensated by the upwelling of nutrients, although
671 seasonality of these fluxes is not in phase (Mdutyana et al., 2020). Here, we focused on the summer season, therefore
672 the net export of nitrogen that we report does not represent an annual flux. However, the model indicates that
673 productivity decreases with deeper mixing, ~~with~~in line with our interpretation of transect data, and this translates to
674 reduced flux of sinking particles in the summer. ~~The inferred primary productivity changes may also have implications~~
675 ~~for the carbon cycle and the biological pump.~~

676 Overall, the model confirms the observations that sea ice seasonality is not the principal control on productivity and
677 surface nitrate drawdown, which are rather tied to summer MLD. The $\delta^{15}N$ of nitrate increases with surface nitrate
678 drawdown, and both vary jointly with net productivity and particulate export.

5. Conclusions

680 We investigated nitrate dynamics near the Antarctic Peninsula in the Southern Ocean, to better understand
681 ~~environmental controls on~~if sea ice impacts primary productivity by analyzing nitrate drawdown. We compiled
682 measurements from different databases and new transects for a total of 394 nitrate profiles. In this region seasonally
683 covered by sea ice, nitrate is not limiting productivity, and remains in concentrations above 20 µmol kg^{-1} at any time
684 of the year. We evaluated the influence of sea ice on nitrate depletion in the surface water, testing the hypothesis that
685 sea ice melting reduces surface salinity and enhances the stratification propitious to primary producers (Taylor et al.,
686 2013). We used nitrate depletion, defined as surface concentration minus concentration in the Winter Water layer, as
687 an indicator of nutrient uptake and net seasonal productivity. Results do not clearly point to a change in nitrate
688 depletion in regions where sea ice duration differs. Significant nitrate depletion is mostly observed after melting,
689 owing to favorable conditions for blooming after ice melt. However, sea ice melting is not necessarily followed by
690 nitrate depletion. Seasonal amplitude of sea ice only marginally affects nitrate depletion and stratification, opposing
691 the hypothesis that sea ice meltwater controls stratification at the regional scale. Diverse oceanographic controls in
692 the water masses properties, density gradients and mixing may mask the impact of sea ice on productivity and nitrate
693 depletion when comparing a variety of locations.

694 Analysis of nitrate along new north-south transects in the DP and Powell basin east of the BS reveals a channel of
695 deeply mixed waters with high surface nitrate concentration. We interpret this channel to be a remnant of actively
696 homogenized water with tidal mixing along the SSI upstream the BS (Zhou et al., 2020). $\delta^{15}N$ of nitrate in these
697 transects confirm the previously established relationship between nitrate drawdown and ^{15}N-enrichment in the
698 remaining nitrate. The strong correlation between logarithm of nitrate concentration and ~~$-$~~$\delta^{15}N$ indicate that the system
699 is well approximated by a Rayleigh distillation, with limited resupply of nitrate during phytoplankton growth.
700 ~~Furthermore, the higher nitrogen isotope effect estimated in the deeply mixed profiles suggests a light limitation during~~
701 ~~nitrate uptake, contributing to the lower nitrate depletion at these locations.~~ Nitrogen isotope modeling further supports
702 that deeper mixing in the BS induces light limitation, with lower nitrate uptake and $\delta^{15}N$ compared to both the DP and
703 the WS. Weaker sinking particle flux in the eastern BS equates to weaker organic matter export in summer.

704 Strong stratification in the summer surface ocean makes nitrate depletion a ~~seasonal lasting~~persistent summertime
705 feature, useful for integrating biological uptake over a growth season. However, variations in MLD ~~makes~~make it
706 difficult to quantify nitrate uptake and productivity based on surface concentration changes alone, ~~but hints towards~~
707 ~~weaker productivity in deeply mixed layer allows the use~~requiring vertical profiles of nitrate ~~concentration for~~
708 ~~qualitative estimates. Nitrate utilization appears tied to the MLD, which hardly depends on sea ice meltwater release.~~
709 ~~Multiple oceanographic features influence the MLD at the regional scale, with varying water masses and mixing~~

710 ~~dynamics affecting vertical density.~~concentrations. Nonetheless, ~~it should be noted~~the consistency of the nitrate data
711 with the Rayleigh model imply that ~~heavily sea-iced areas~~there were ~~was~~ not a strong resupply of nitrate late in the
712 summer season, such that surface nitrate concentration changes are ~~comparatively under-sampled, and future efforts~~
713 ~~may be oriented to fill this knowledge gap.~~a plausible indicator of spring-summer nitrate assimilation..

714 Increasing temperatures with global climate change will likely reduce the extent of sea ice in the future. Summer
715 stratification could shift from a salinity-based density gradient to a temperature-based density gradient. This will
716 probably impact phytoplanktonic activity and ecosystems in a warmer surface layer with a longer ice-free season. A
717 supposed decrease in freshwater supply in the surface ocean would tend to increase MLD inducing light limitation on
718 phytoplanktonic productivity, but this would be counterbalanced by increased productivity in warmer waters and
719 longer growth season. Determining which of these two effects prevails is crucial to understand future changes in the
720 phytoplankton productivity of the high latitude Southern Ocean.

721

722 **Appendix A: Station-specific profiles and isotope effect**

723
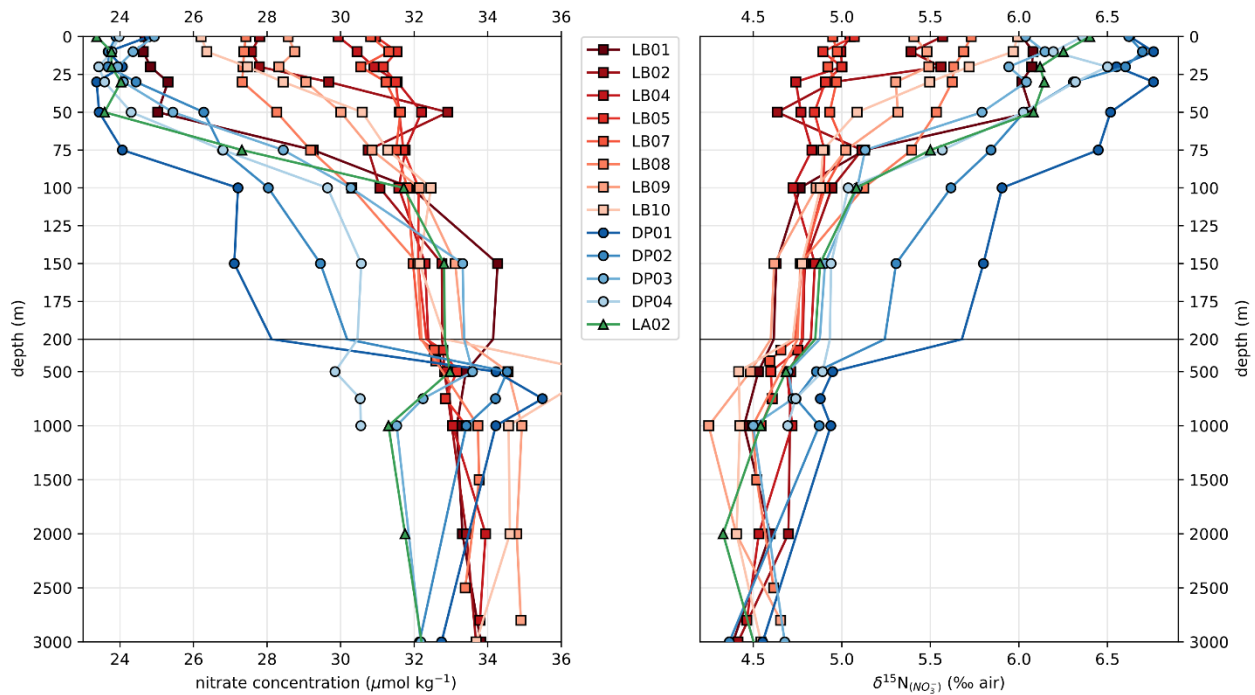
724 **Figure A1. Station-specific profiles of (a) nitrate concentration and (b) δ^{15}N of nitrate.**

26

726
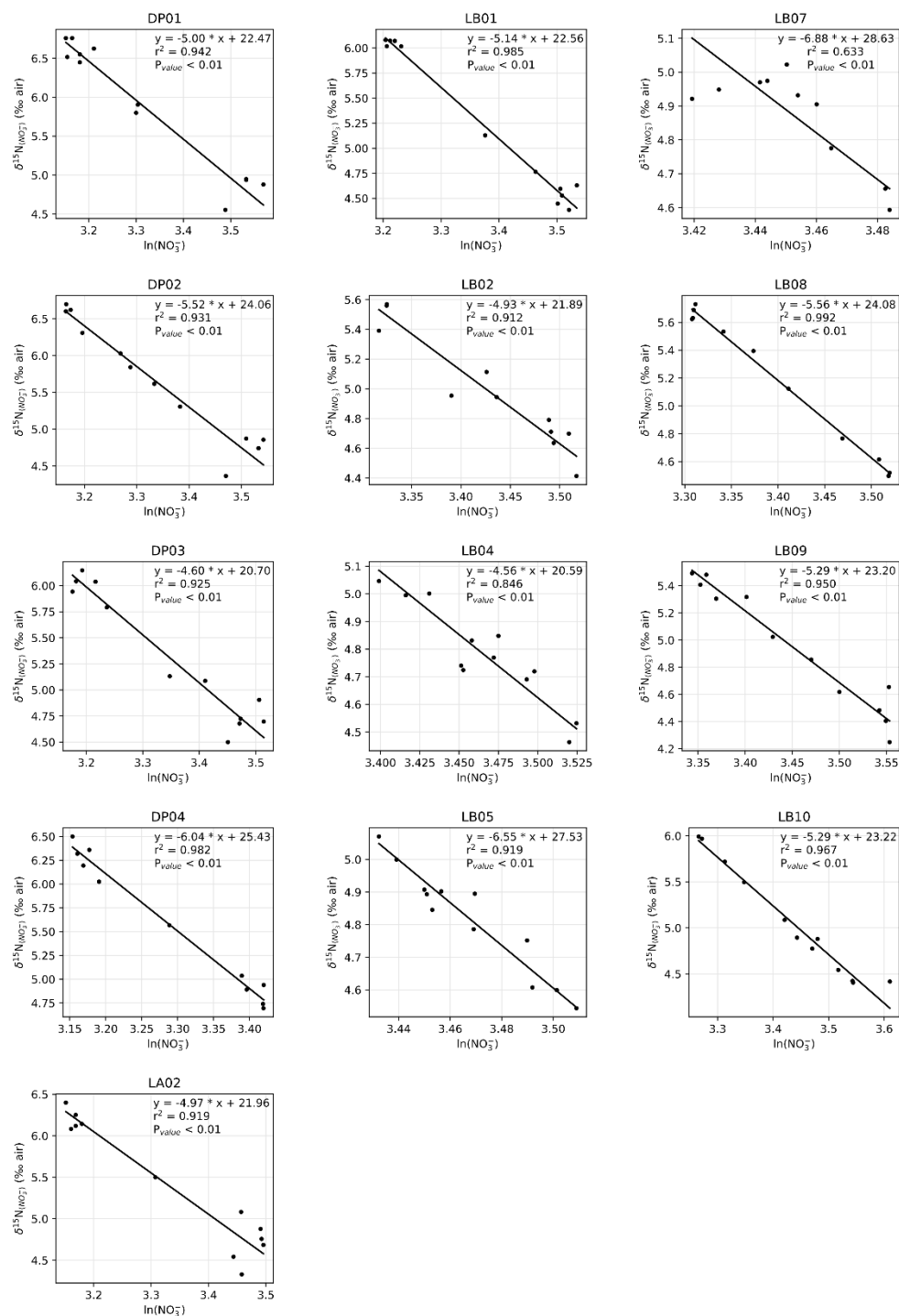
Figure A2. δ^{15}N of nitrate as a function of nitrate concentration (logarithmic scale) for each KARP-20 profile, used for estimation of nitrate isotope effect ε (opposite of the slope value, Eq. (1)).

Code availability

27

Python code for data processing and figure creation is available on a Zenodo repository (doi:10.5281/zenodo.14221104) for transparency and reproducibility purposes. Potential users should know that it was developed for personal use and has not been cleaned up before distribution. Nitrogen cycle model inquiries should be sent to C. Yoshikawa (yoshikawac@jamstec.go.jp).

Data availability

Sample availability

Samples from this study are not available.

Author contribution

Concept of the study, formal analysis and figure creation were conducted by APMS, as part of project co-led by FJJE and NO. The nitrogen model was developed by CY. Water samples were collected by YJ and BKK. Nitrogen data was obtained and curated by YJ, BKK, YR and DMS at Princeton university. The original manuscript prepared by APMS, YI, and CY, with revisions from BKK, NOO, YR, FJJE and NO.

Competing interests

The authors declare that they have no conflict of interest.

Acknowledgements

Financial Support

References

Altabet, M. A.: Isotopic Tracers of the Marine Nitrogen Cycle: Present and Past, in: Marine Organic Matter: Biomarkers, Isotopes and DNA, edited by: Volkman, J. K., Springer, Berlin, Heidelberg, 251–293, https://doi.org/10.1007/698_2_008, 2006.

Altabet, M. A. and Francois, R.: Nitrogen isotope biogeochemistry of the Antarctic Polar Frontal Zone at 170°W, Deep Sea Research Part II: Topical Studies in Oceanography, 48, 4247–4273, https://doi.org/10.1016/S0967-0645(01)00088-1, 2001.

Annett, A. L., Fitzsimmons, J. N., Séguret, M. J. M., Lagerström, M., Meredith, M. P., Schofield, O., and Sherrell, R. M.: Controls on dissolved and particulate iron distributions in surface waters of the Western Antarctic Peninsula shelf, Marine Chemistry, 196, 81–97, https://doi.org/10.1016/j.marchem.2017.06.004, 2017.

Aoyama, M.: Global certified-reference-material- or reference-material-scaled nutrient gridded dataset GND13, Earth System Science Data, 12, 487–499, https://doi.org/10.5194/essd-12-487-2020, 2020.

Ardelan, M. V., Holm-Hansen, O., Hewes, C. D., Reiss, C. S., Silva, N. S., Dulaiova, H., Steinnes, E., and Sakshaug, E.: Natural iron enrichment around the Antarctic Peninsula in the Southern Ocean, Biogeosciences, 7, 11–25, https://doi.org/10.5194/bg-7-11-2010, 2010.

Armstrong, F. A. J., Stearns, C. R., and Strickland, J. D. H.: The measurement of upwelling and subsequent biological process by means of the Technicon Autoanalyzer® and associated equipment, Deep Sea Research and Oceanographic Abstracts, 14, 381–389, https://doi.org/10.1016/0011-7471(67)90082-4, 1967.

Arrigo, K. R.: Sea ice as a habitat for primary producers, in: Sea Ice, John Wiley & Sons, Ltd, 352–369, https://doi.org/10.1002/9781118778371.ch14, 2017.

Arrigo, K. R., Worthen, D., Schnell, A., and Lizotte, M. P.: Primary production in Southern Ocean waters, Journal of Geophysical Research: Oceans, 103, 15587–15600, https://doi.org/10.1029/98JC00930, 1998.

Arrigo, K. R., van Dijken, G. L., and Bushinsky, S.: Primary production in the Southern Ocean, 1997–2006, Journal of Geophysical Research: Oceans, 113, C08004, https://doi.org/10.1029/2007JC004551, 2008.

Arteaga, L. A., Boss, E., Behrenfeld, M. J., Westberry, T. K., and Sarmiento, J. L.: Seasonal modulation of phytoplankton biomass in the Southern Ocean, Nat Commun, 11, 5364, https://doi.org/10.1038/s41467-020-19157-2, 2020.

Behera, N., Swain, D., and Sil, S.: Effect of Antarctic sea ice on chlorophyll concentration in the Southern Ocean, Deep Sea Research Part II: Topical Studies in Oceanography, 178, 104853, https://doi.org/10.1016/j.dsr2.2020.104853, 2020.

Bélanger, S., Ehn, J. K., and Babin, M.: Impact of sea ice on the retrieval of water-leaving reflectance, chlorophyll a concentration and inherent optical properties from satellite ocean color data, Remote Sensing of Environment, 111, 51–68, https://doi.org/10.1016/j.rse.2007.03.013, 2007.

Bode, A., Castro, C. G., Doval, M. D., and Varela, M.: New and regenerated production and ammonium regeneration in the western Bransfield Strait region (Antarctica) during phytoplankton bloom conditions in summer, Deep Sea Research Part II: Topical Studies in Oceanography, 49, 787–804, doi:10.1016/S0967-0645(01)00124-2, 2002.

von Berg, L., Prend, C. J., Campbell, E. C., Mazloff, M. R., Talley, L. D., and Gille, S. T.: Weddell Sea Phytoplankton Blooms Modulated by Sea Ice Variability and Polynya Formation, Geophysical Research Letters, 47, e2020GL087954, https://doi.org/10.1029/2020GL087954, 2020.

Boyd, P. W. and Ellwood, M. J.: The biogeochemical cycle of iron in the ocean, Nature Geosci, 3, 675–682, https://doi.org/10.1038/ngeo964, 2010.

de Boyer Montégut, C., Madec, G., Fischer, A. S., Lazar, A., and Iudicone, D.: Mixed layer depth over the global ocean: An examination of profile data and a profile-based climatology, Journal of Geophysical Research: Oceans, 109, C12003, https://doi.org/10.1029/2004JC002378, 2004.

Braman, R. S. and Hendrix, S. A.: Nanogram nitrite and nitrate determination in environmental and biological materials by vanadium(III) reduction with chemiluminescence detection, Anal. Chem., 61, 2715–2718, https://doi.org/10.1021/ac00199a007, 1989.

Briggs, E. M., Martz, T. R., Talley, L. D., Mazloff, M. R., and Johnson, K. S.: Physical and Biological Drivers of Biogeochemical Tracers Within the Seasonal Sea Ice Zone of the Southern Ocean From Profiling Floats, Journal of Geophysical Research: Oceans, 123, 746–758, https://doi.org/10.1002/2017JC012846, 2018.

Castro, C. G., Ríos, A. F., Doval, M. D., and Pérez, F. F.: Nutrient utilisation and chlorophyll distribution in the Atlantic sector of the Southern Ocean during Austral summer 1995–96, Deep Sea Research Part II: Topical Studies in Oceanography, 49, 623–641, https://doi.org/10.1016/S0967-0645(01)00115-1, 2002.

Codispoti, L. A., Kelly, V., Thessen, A., Matrai, P., Suttles, S., Hill, V., Steele, M., and Light, B.: Synthesis of primary production in the Arctic Ocean: III. Nitrate and phosphate based estimates of net community production, Progress in Oceanography, 110, 126–150, https://doi.org/10.1016/j.pocean.2012.11.006, 2013.

~~DeVries~~DiFiore, P. J., Sigman, D. M., Trull, T.~~, Primeau, F.,~~ W., Lourey, M. J., Karsh, K., Cane, G., and ~~Deutsch, C.: The sequestration efficiency~~Ho, R.: Nitrogen isotope constraints on subantarctic biogeochemistry, Journal ~~of the biological pump,~~ Geophysical Research ~~Letters, 39, L13601,~~: Oceans, 111, C08016, https://doi.org/10.1029/~~2012GL051963, 2012~~2005JC003216, 2006.

DiFiore, P. J., Sigman, D. M., and Dunbar, R. B.: Upper ocean nitrogen fluxes in the Polar Antarctic Zone: Constraints from the nitrogen and oxygen isotopes of nitrate, Geochemistry, Geophysics, Geosystems, 10, Q11016, https://doi.org/10.1029/2009GC002468, 2009.

DiFiore, P. J., Sigman, D. M., Karsh, K. L., Trull, T. W., Dunbar, R. B., and Robinson, R. S.: Poleward decrease in the isotope effect of nitrate assimilation across the Southern Ocean, Geophysical Research Letters, 37, L17601, https://doi.org/10.1029/2010GL044090, 2010.

Fahrbach, E.: Cruise Report for R/V Polarstern Expedition 06AQANTX_7 on WOCE section SR04, ~~CLIVAR and Carbon Hydrographic Data Office,~~ https://cchdo.ucsd.edu/cruise/06AQANTX_7, 1993.

Fan, T., Deser, C., and Schneider, D. P.: Recent Antarctic sea ice trends in the context of Southern Ocean surface climate variations since 1950, Geophysical Research Letters, 41, 2419–2426, https://doi.org/10.1002/2014GL059239, 2014.

Flynn, R. F., Bornman, T. G., Burger, J. M., Smith, S., Spence, K. A. M., and Fawcett, S. E.: Summertime productivity and carbon export potential in the Weddell Sea, with a focus on the waters adjacent to Larsen C Ice Shelf, Biogeosciences, 18, 6031–6059, https://doi.org/10.5194/bg-18-6031-2021, 2021.

Franck, V. M., Brzezinski, M. A., Coale, K. H., and Nelson, D. M.: Iron and silicic acid concentrations regulate Si uptake north and south of the Polar Frontal Zone in the Pacific Sector of the Southern Ocean, Deep Sea Research Part II: Topical Studies in Oceanography, 47, 3315–3338, https://doi.org/10.1016/S0967-0645(00)00070-9, 2000.

Frants, M., Gille, S. T., Hatta, M., Hiscock, W. T., Kahru, M., Measures, C. I., Greg Mitchell, B., and Zhou, M.: Analysis of horizontal and vertical processes contributing to natural iron supply in the mixed layer in southern Drake Passage, Deep Sea Research Part II: Topical Studies in Oceanography, 90, 68–76, https://doi.org/10.1016/j.dsr2.2012.06.001, 2013.

Frey, D. I., Krechik, V. A., Morozov, E. G., Drozd, I. D., Gordey, A. S., Latushkin, A. A., Mekhova, O. S., Mukhametianov, R. Z., Murzina, S. A., Ostroumova, S. A., Ponomarev, V. I., Salyuk, P. A., Smirnova, D. A., Shutov, S. A., and Zuev, O. A.: Water Exchange between Deep Basins of the Bransfield Strait, Water, 14, 3193, https://doi.org/10.3390/w14203193, 2022.

Fripiat, F., Sigman, D. M., Fawcett, S. E., Rafter, P. A., Weigand, M. A., and Tison, J.-L.: New insights into sea ice nitrogen biogeochemical dynamics from the nitrogen isotopes, Global Biogeochemical Cycles, 28, 115–130, https://doi.org/10.1002/2013GB004729, 2014.

852 Fripiat, F., Elskens, M., Trull, T. W., Blain, S., Cavagna, A.-J., Fernandez, C., Fonseca-Batista, D., Planchon, F.,
853 Raimbault, P., Roukaerts, A., and Dehairs, F.: Significant mixed layer nitrification in a natural iron-fertilized bloom
854 of the Southern Ocean, Global Biogeochemical Cycles, 29, 1929–1943, https://doi:.org/10.1002/2014GB005051,
855 2015.

856 Fripiat, F., Martínez-García, A., Fawcett, S. E., Kemeny, P. C., Studer, A. S., Smart, S. M., Rubach, F., Oleynik, S.,
857 Sigman, D. M., and Haug, G. H.: The isotope effect of nitrate assimilation in the Antarctic Zone: Improved estimates
858 and paleoceanographic implications, Geochimica et Cosmochimica Acta, 247, 261–279,
859 https://doi.org/10.1016/j.gca.2018.12.003, 2019.

860 Garcia, H. E., Boyer, T. P., Baranova, O. K., Locarnini, R. A., Mishonov, A. V., Grodsky, A., Paver, C. R., Weathers,
861 K. W., Smolyar, I. V., Reagan, J. R., Seidov, D., and Zweng, M. M.: World Ocean Atlas 2018 [data set],
862 https://www.ncei.noaa.gov/data/oceans/woa/WOA18/, 2019. [Accessed July 2023]

863 Goeyens, L., Tréguer, P., Baumann, M. E. M., Baeyens, W., and Dehairs, F.: The leading role of ammonium in the
864 nitrogen uptake regime of Southern Ocean marginal ice zones, Journal of Marine Systems, 6, 345–361,
865 https://doi:.org/10.1016/0924-7963(94)00033-8, 1995.

866 Gonçalves-Araujo, R., De Souza, M. S., Tavano, V. M., and Garcia, C. A. E.: Influence of oceanographic features on
867 spatial and interannual variability of phytoplankton in the Bransfield Strait, Antarctica, Journal of Marine Systems,
868 142, 1–15, https://doi:.org/10.1016/j.jmarsys.2014.09.007, 2015.

869 Gordon, A. L., Mensch, M., Zhaoqian, D., Smethie, W. M., and de Bettencourt, J.: Deep and bottom water of the
870 Bransfield Strait eastern and central basins, J. Geophys. Res., 105, 11337–11346,
871 https://doi:.org/10.1029/2000JC900030, 2000.

872 Gruber, N., Gloor, M., Mikaloff Fletcher, S. E., Doney, S. C., Dutkiewicz, S., Follows, M. J., Gerber, M., Jacobson,
873 A. R., Joos, F., Lindsay, K., Menemenlis, D., Mouchet, A., Müller, S. A., Sarmiento, J. L., and Takahashi, T.: Oceanic
874 sources, sinks, and transport of atmospheric CO2, Global Biogeochemical Cycles, 23, GB1005,
875 doi:10.1029/2008GB003349, 2009.

876 Hatta, M., Measures, C. I., Selph, K. E., Zhou, M., and Hiscock, W. T.: Iron fluxes from the shelf regions near the
877 South Shetland Islands in the Drake Passage during the austral-winter 2006, Deep Sea Research Part II: Topical
878 Studies in Oceanography, 90, 89–101, https://doi:.org/10.1016/j.dsr2.2012.11.003, 2013.

879 Huang, Y. and Fassbender, A. J.: Biological Production of Distinct Carbon Pools Drives Particle Export Efficiency in
880 the Southern Ocean, Geophysical Research Letters, 51, e2023GL107511, doi:10.1029/2023GL107511, 2024.

881 Huneke, W. G. C., Huhn, O., and Schröeder, M.: Water masses in the Bransfield Strait and adjacent seas, austral
882 summer 2013, Polar Biol, 39, 789–798, https://doi:.org/10.1007/s00300-016-1936-8, 2016.

883 Jiang, M., Measures, C. I., Barbeau, K. A., Charette, M. A., Gille, S. T., Hatta, M., Kahru, M., Mitchell, B. G., Naveira
884 Garabato, A. C., Reiss, C., Selph, K., and Zhou, M.: Fe sources and transport from the Antarctic Peninsula shelf to
885 the southern Scotia Sea, Deep Sea Research Part I: Oceanographic Research Papers, 150, 103060,
886 https://doi:.org/10.1016/j.dsr.2019.06.006, 2019.

887 Johnson, K. S. and Coletti, L. J.: In situ ultraviolet spectrophotometry for high resolution and long-term monitoring
888 of nitrate, bromide and bisulfide in the ocean, Deep Sea Research Part I: Oceanographic Research Papers, 49, 1291–
889 1305, https://doi:.org/10.1016/S0967-0637(02)00020-1, 2002.

890 Johnson, K. S., Coletti, L. J., Jannasch, H. W., Sakamoto, C. M., Swift, D. D., and Riser, S. C.: Long-Term Nitrate
891 Measurements in the Ocean Using the in situ Ultraviolet Spectrophotometer: Sensor Integration into the APEX
892 Profiling Float, Journal of Atmospheric and Oceanic Technology, 30, 1854–1866, https://doi:.org/10.1175/JTECH-
893 D-12-00221.1, 2013.

Johnson, K. S., Plant, J. N., Coletti, L. J., Jannasch, H. W., Sakamoto, C. M., Riser, S. C., Swift, D. D., Williams, N. L., Boss, E., Haëntjens, N., Talley, L. D., and Sarmiento, J. L.: Biogeochemical sensor performance in the SOCCOM profiling float array, Journal of Geophysical Research: Oceans, 122, 6416–6436, https://doi:.org/10.1002/2017JC012838, 2017.

Jones, J. M., Gille, S. T., Goosse, H., Abram, N. J., Canziani, P. O., Charman, D. J., Clem, K. R., Crosta, X., de Lavergne, C., Eisenman, I., England, M. H., Fogt, R. L., Frankcombe, L. M., Marshall, G. J., Masson-Delmotte, V., Morrison, A. K., Orsi, A. J., Raphael, M. N., Renwick, J. A., Schneider, D. P., Simpkins, G. R., Steig, E. J., Stenni, B., Swingedouw, D., and Vance, T. R.: Assessing recent trends in high-latitude Southern Hemisphere surface climate, Nature Clim Change, 6, 917–926, https://doi:.org/10.1038/nclimate3103, 2016.

Kalnay, E., Kanamitsu, M., Kistler, R., Collins, W., Deaven, D., Gandin, L., Iredell, M., Saha, S., White, G., Woollen, J., Zhu, Y., Chelliah, M., Ebisuzaki, W., Higgins, W., Janowiak, J., Mo, K. C., Ropelewski, C., Wang, J., Leetmaa, A., Reynolds, R., Jenne, R., and Joseph, D.: The NCEP/NCAR 40-Year Reanalysis Project, Bulletin of the American Meteorological Society, 77, 437–472, https://doi:.org/10.1175/1520-0477(1996)077<0437:TNYRP>2.0.CO;2, 1996.

Kemeny, P. C., Weigand, M. A., Zhang, R., Carter, B. R., Karsh, K. L., Fawcett, S. E., and Sigman, D. M.: Enzyme-level interconversion of nitrate and nitrite in the fall mixed layer of the Antarctic Ocean, Global Biogeochemical Cycles, 30, 1069–1085, https://doi.org/10.1002/2015GB005350, 2016.

Key, R. M., Olsen, A., van Heuven, S., Lauvset, S. K., Velo, A., Lin, X., Schirnick, C., Kozyr, A., Tanhua, T., Hoppema, M., Jutterström, S., Steinfeldt, R., Jeansson, E., Ishii, M., Perez, F. F., and Suzuki, T.: Global Ocean Data Analysis Project, Version 2 (GLODAPv2), Ornl/Cdiac 162, Ndp 093, 8:297 323, doi:https://doi.org/doi:10.3334/CDIAC/OTG.NDP093_GLODAPv2, 2015.

Klunder, M. B., Laan, P., De Baar, H. J. W., Middag, R., Neven, I., and Van Ooijen, J.: Dissolved Fe across the Weddell Sea and Drake Passage: impact of DFe on nutrient uptake, Biogeosciences, 11, 651–669, https://doi.org/10.5194/bg-11-651-2014, 2014.

Kwok, R. and Kacimi, S.: Three years of sea ice freeboard, snow depth, and ice thickness of the Weddell Sea from Operation IceBridge and CryoSat-2, The Cryosphere, 12, 2789–2801, https://doi:.org/10.5194/tc-12-2789-2018, 2018.

La, H. S., Park, K., Chae, J. Y., Park, T., and Park, J.: Climatic factors and their robust evidences controlling phytoplankton biomass in the Bransfield Strait, Terr. Atmos. Ocean. Sci., 30, 821–830, https://doi:.org/10.3319/TAO.2019.04.30.01, 2019.

Lannuzel, D., Vancoppenolle, M., van der Merwe, P., de Jong, J., Meiners, K. M., Grotti, M., Nishioka, J., and Schoemann, V.: Iron in sea ice: Review and new insights, Elementa: Science of the Anthropocene, 4, 000130, https://doi.org/10.12952/journal.elementa.000130, 2016.

Lauvset, S. K., Lange, N., Tanhua, T., Bittig, H. C., Olsen, A., Kozyr, A., Alin, S., Álvarez, M., Azetsu-Scott, K., Barbero, L., Becker, S., Brown, P. J., Carter, B. R., da Cunha, L. C., Feely, R. A., Hoppema, M., Humphreys, M. P., Ishii, M., Jeansson, E., Jiang, L.-Q., Jones, S. D., Lo Monaco, C., Murata, A., Müller, J. D., Pérez, F. F., Pfeil, B., Schirnick, C., Steinfeldt, R., Suzuki, T., Tilbrook, B., Ulfsbo, A., Velo, A., Woosley, R. J., and Key, R. M.: GLODAPv2.2022: the latest version of the global interior ocean biogeochemical data product, Earth System Science Data, 14, 5543–5572, https://doi:.org/10.5194/essd-14-5543-2022, 2022.

Lavergne, T., Sørensen, A. M., Kern, S., Tonboe, R., Notz, D., Aaboe, S., Bell, L., Dybkjær, G., Eastwood, S., Gabarro, C., Heygster, G., Killie, M. A., Brandt Kreiner, M., Lavelle, J., Saldo, R., Sandven, S., and Pedersen, L. T.: Version 2 of the EUMETSAT OSI SAF and ESA CCI sea-ice concentration climate data records, The Cryosphere, 13, 49–78, https://doi:.org/10.5194/tc-13-49-2019, 2019.

Lavergne, T., Sørensen, A., Tonboe, R., Strong, C., Kreiner, M., Saldo, R., Birkedal, A., Baordo, F., Rusin, J., Aspenes, T., and Eastwood, S.: Monitoring of Sea Ice Concentration, Area, and Extent in the polar regions : 40+ years of data

937 from EUMETSAT OSI SAF and ESA CCI, IAF Global Space Conference on Climate Change (GLOC 2023),, Oslo,
938 Norway, 23-25 May 2023, GLOC-2023,T,1,7,x75079, https://doi:.org/10.5281/zenodo.10014534, 2023.

939 Lewis, M. R., Hebert, D., Harrison, W. G., Platt, T., and Oakey, N. S.: Vertical Nitrate Fluxes in the Oligotrophic
940 Ocean, Science, 234, 870–873, https://doi:.org/10.1126/science.234.4778.870, 1986.

941 Lourey, M. J. and Trull, T. W.: Seasonal nutrient depletion and carbon export in the Subantarctic and Polar Frontal
942 zones of the Southern Ocean south of Australia, Journal of Geophysical Research: Oceans, 106, 31463–31487,
943 https://doi.org/10.1029/2000JC000287, 2001.

944 Lourey, M. J., Trull, T. W., and Sigman, D. M.: Sensitivity of δ^{15}N of nitrate, surface suspended and deep sinking
945 particulate nitrogen to seasonal nitrate depletion in the Southern Ocean, Global Biogeochem. Cycles, 17, 1081,
946 https://doi:.org/10.1029/2002GB001973, 2003.

947 Franck, V. M., Brzezinski, M. A., Coale, K. H., and Nelson, D. M.: Iron and silicic acid concentrations regulate Si
948 uptake north and south of the Polar Frontal Zone in the Pacific Sector of the Southern Ocean, Deep Sea Research Part
949 II: Topical Studies in Oceanography, 47, 3315–3338, doi:10.1016/S0967-0645(00)00070-9, 2000.

950 MacIntyre, G., Plache, B., Lewis, M. R., Andrea, J., Feener, S., McLean, S. D., Johnson, K. S., Coletti, L. J., and
951 Jannasch, H. W.: ISUS/SUNA nitrate measurements in networked ocean observing systems, in: OCEANS 2009,
952 OCEANS 2009, Biloxi, MS, 1–7, https://doi:.org/10.23919/OCEANS.2009.5422251, 2009.

953 Mariotti, A., Germon, J. C., Hubert, P., Kaiser, P., Letolle, R., Tardieux, A., and Tardieux, P.: Experimental
954 determination of nitrogen kinetic isotope fractionation: Some principles; illustration for the denitrification and
955 nitrification processes, Plant Soil, 62, 413–430, https://doi:.org/10.1007/BF02374138, 1981.

956 Marshall, J. and Speer, K.: Closure of the meridional overturning circulation through Southern Ocean upwelling,
957 Nature Geosci, 5, 171–180, https://doi.org/10.1038/ngeo1391, 2012.

958 Maurer, T. L., Plant, J. N., and Johnson, K. S.: Delayed-Mode Quality Control of Oxygen, Nitrate, and pH Data on
959 SOCCOM Biogeochemical Profiling Floats, Front. Mar. Sci., 8, 683207, https://doi:.org/10.3389/fmars.2021.683207,
960 2021.

961 Mdutyana, M., Thomalla, S. J., Philibert, R., Ward, B. B., and Fawcett, S. E.: The Seasonal Cycle of Nitrogen Uptake
962 and Nitrification in the Atlantic Sector of the Southern Ocean, Global Biogeochemical Cycles, 34, e2019GB006363,
963 https://doi:.org/10.1029/2019GB006363, 2020.

964 Measures, C. I., Brown, M. T., Selph, K. E., Apprill, A., Zhou, M., Hatta, M., and Hiscock, W. T.: The influence of
965 shelf processes in delivering dissolved iron to the HNLC waters of the Drake Passage, Antarctica, Deep Sea Research
966 Part II: Topical Studies in Oceanography, 90, 77–88, https://doi:.org/10.1016/j.dsr2.2012.11.004, 2013.

967 Mengesha, S., Dehairs, F., Fiala, M., Elskens, M., and Goeyens, L.: Seasonal variation of phytoplankton community
968 structure and nitrogen uptake regime in the Indian Sector of the Southern Ocean, Polar Biol, 20, 259–272,
969 https://doi:.org/10.1007/s003000050302, 1998.

970 Moffat, C. and Meredith, M.: Shelf–ocean exchange and hydrography west of the Antarctic Peninsula: a review, Phil.
971 Trans. R. Soc. A., 376, 20170164, https://doi:.org/10.1098/rsta.2017.0164, 2018.

972 Moline, M. and Prézelin, B.: Long-term monitoring and analyses of physical factors regulating variability in coastal
973 Antarctic phytoplankton biomass, in situ productivity and taxonomic composition over subseasonal, seasonal and
974 interannual time scales, Mar. Ecol. Prog. Ser., 145, 143–160, https://doi:.org/10.3354/meps145143, 1996.

975 Moore, J. K., Doney, S. C., Glover, D. M., and Fung, I. Y.: Iron cycling and nutrient-limitation patterns in surface
976 waters of the World Ocean, 49, 463––507, https://doi:.org/doi.org/10.1016/S0967-0645(01)00109-6, 2002.

Moreau, S., Mostajir, B., Bélanger, S., Schloss, I. R., Vancoppenolle, M., Demers, S., and Ferreyra, G. A.: Climate change enhances primary production in the western Antarctic Peninsula, Global Change Biology, 21, 2191–2205, https://doi.org/10.1111/gcb.12878, 2015.

Moreau, S., Boyd, P. W., and Strutton, P. G.: Remote assessment of the fate of phytoplankton in the Southern Ocean sea-ice zone, Nat Commun, 11, 3108, https://doi.org/10.1038/s41467-020-16931-0, 2020.

Morrison, A. K., Frölicher, T. L., and Sarmiento, J. L.: Upwelling in the Southern Ocean, Physics Today, 68, 27–32, https://doi.org/10.1063/PT.3.2654, 2015.

Needoba, J. A. and Harrison, P. J.: INFLUENCE OF LOW LIGHT AND A LIGHT: DARK CYCLE ON NO$_3^-$ UPTAKE, INTRACELLULAR NO$_3^-$, AND NITROGEN ISOTOPE FRACTIONATION BY MARINE PHYTOPLANKTON, Journal of Phycology, 40, 505–516, https://doi.org/10.1111/j.1529-8817.2004.03171.x, 2004.

Needoba, J. A., Sigman, D. M., and Harrison, P. J.: THE MECHANISM OF ISOTOPE FRACTIONATION DURING ALGAL NITRATE ASSIMILATION AS ILLUMINATED BY THE ^{15}N/-^{14}N OF INTRACELLULAR NITRATE, Journal of Phycology, 40, 517–522, https://doi.org/10.1111/j.1529-8817.2004.03172.x, 2004.

Nelson, D. M., Anderson, R. F., Barber, R. T., Brzezinski, M. A., Buesseler, K. O., Chase, Z., Collier, R. W., Dickson, M.-L., François, R., Hiscock, M. R., Honjo, S., Marra, J., Martin, W. R., Sambrotto, R. N., Sayles, F. L., and Sigmon, D. E.: Vertical budgets for organic carbon and biogenic silica in the Pacific sector of the Southern Ocean, 1996–1998, Deep Sea Research Part II: Topical Studies in Oceanography, 49, 1645–1674, https://doi.org/10.1016/S0967-0645(02)00005-X, 2002.

NOAA National Centers for Environmental Information: ETOPO 2022 15 Arc-Second Global Relief Model [data set], https://doi.org/10.25921/fd45-gt74, 2022. [Accessed 2023-05-08]

Ohkouchi, N. and Takano, Y.: Organic Nitrogen: Sources, Fates, and Chemistry, in: Treatise on Geochemistry, vol. 12, edited by: Holland, H. D. and Turekian, K. K., Elsevier, 251–289, https://doi.org/10.1016/B978-0-08-095975-7.01015-9, 2014.

Olsen, A., Key, R. M., van Heuven, S., Lauvset, S. K., Velo, A., Lin, X., Schirnick, C., Kozyr, A., Tanhua, T., Hoppema, M., Jutterström, S., Steinfeldt, R., Jeansson, E., Ishii, M., Pérez, F. F., and Suzuki, T.: The Global Ocean Data Analysis Project version 2 (GLODAPv2) – an internally consistent data product for the world ocean, Earth System Science Data, 8, 297–323, https://doi.org/10.5194/essd-8-297-2016, 2016.

OSI SAF: Global Sea Ice Concentration Climate Data Record v3.0 - Multimission, EUMETSAT SAF on Ocean and Sea Ice [data set], https://doi.org/10.15770/EUM_SAF_OSI_0013, 2022a. [Accessed 2023-09-07]

OSI SAF: Global Sea Ice Concentration Interim Climate Data Record Release 3 - DMSP, EUMETSAT SAF on Ocean and Sea Ice [data set], https://doi.org/10.15770/EUM_SAF_OSI_0014, 2022b. [Accessed 2023-09-07]

Parkinson, C. L. and Cavalieri, D. J.: Antarctic sea ice variability and trends, 1979–2010, The Cryosphere, 6, 871–880, https://doi.org/10.5194/tc-6-871-2012, 2012.

Pellichero, V., Sallée, J.-B., Schmidtko, S., Roquet, F., and Charrassin, J.-B.: The ocean mixed layer under Southern Ocean sea-ice: Seasonal cycle and forcing, Journal of Geophysical Research: Oceans, 122, 1608–1633, https://doi.org/10.1002/2016JC011970, 2017.

Pollard, R. T., Rhines, P. B., and Thompson, R. O. R. Y.: The deepening of the wind-Mixed layer, Geophysical Fluid Dynamics, 4, 381–404, https://doi.org/10.1080/03091927208236105, 1973.

Prend, C. J., Keerthi, M. Pondaven, P., RagueneauG., Lévy, M., Aumont, O., Gille, S. TTréguer, P., Hauvespre, A., Dezileau, L., and Talley, L. D.: Sub-Seasonal Forcing Drives Year-To-Year Variations of Reyss, J. L.: Resolving the 'opal paradox' in the Southern Ocean Primary Productivity, Global Biogeochemical Cycles, 36, e2022GB007329, , Nature, 405, 168–172, https://doi.org/10.1038/35012046, 2000.

Romanova, N. D., Mosharov, S. A., Vorobieva, O. V., and Bardyukova, E. V.: Quantitative and Productional Characteristics of Microplankton in the Powell Basin and Bransfield Strait in Summer, in: Antarctic Peninsula Region of the Southern Ocean: Oceanography and Ecology, edited by: Morozov, E. G., ~~1029/2022GB007329, 2022~~Flint, M. V., and Spiridonov, V. A., Springer International Publishing, Cham, 197–207, https://doi.org/10.1007/978-3-030-78927-5_14, 2021.

Russo, A. D.~~' A.~~ P. G., de Souza, M. S., Borges Mendes, C. R., Maria Tavano, V., and Eiras Garcia, C. A.: Spatial variability of photophysiology and primary production rates of the phytoplankton communities across the western Antarctic Peninsula in late summer 2013, Deep Sea Research Part II: Topical Studies in Oceanography, 149, 99–110, https://doi.org/10.1016/j.dsr2.2017.09.021, 2018.

~~Sabine, C. L., Feely, R. A., Gruber, N., Key, R. M., Lee, K., Bullister, J. L., Wanninkhof, R., Wong, C. S., Wallace, D. W. R., Tilbrook, B., Millero, F. J., Peng, T.-H., Kozyr, A., Ono, T., and Rios, A. F.: The Oceanic Sink for Anthropogenic CO2, Science, 305, 367–371, doi:10.1126/science.1097403, 2004.~~

Sallée, J. B., Speer, K. G., and Rintoul, S. R.: Zonally asymmetric response of the Southern Ocean mixed-layer depth to the Southern Annular Mode, Nature Geosci, 3, 273–279, https://doi.org/10.1038/ngeo812, 2010.

Sambrotto, R. N. and Mace, B. J.: Coupling of biological and physical regimes across the Antarctic Polar Front as reflected by nitrogen production and recycling, Deep Sea Research Part II: Topical Studies in Oceanography, 47, 3339–3367, https://doi.org/10.1016/S0967-0645(00)00071-0, 2000.

Sangrà, P., Gordo, C., Hernández-Arencibia, M., Marrero-Díaz, A., Rodríguez-Santana, A., Stegner, A., Martínez-Marrero, A., Pelegrí, J. L., and Pichon, T.: The Bransfield current system, Deep Sea Research Part I: Oceanographic Research Papers, 58, 390–402, https://doi.org/10.1016/j.dsr.2011.01.011, 2011.

Savidge, G., Priddle, J., Gilpin, L. C., Bathmann, U., Murphy, E. J., Owens, N. J. P., Pollard, R. T., Turner, D. R., Veth, C., and Boyd, P.: An assessment of the role of the marginal ice zone in the carbon cycle of the Southern Ocean, Antarctic Science, 8, 349–358, https://doi.org/10.1017/S0954102096000521, 1996.

Savoye, N., Dehairs, F., Elskens, M., Cardinal, D., Kopczyńska, E. E., Trull, T. W., Wright, S., Baeyens, W., and Griffiths, F. B.: Regional variation of spring N-uptake and new production in the Southern Ocean, Geophysical Research Letters, 31, L03301, https://doi.org/10.1029/2003GL018946, 2004.

Sherrell, R. M., Annett, A. L., Fitzsimmons, J. N., Roccanova, V. J., and Meredith, M. P.: A 'shallow bathtub ring' of local sedimentary iron input maintains the Palmer Deep biological hotspot on the West Antarctic Peninsula shelf, Philosophical Transactions of the Royal Society A: Mathematical, Physical and Engineering Sciences, 376, 20170171, https://doi.org/10.1098/rsta.2017.0171, 2018.

Sigman, D. M. and Fripiat, F.: Nitrogen Isotopes in the Ocean, in: Encyclopedia of Ocean Sciences, vol. 1, edited by: Cochran, J. K., Bokuniewicz, H. J., and Yager, P. L., Elsevier, 263–278, https://doi.org/10.1016/B978-0-12-409548-9.11605-7, 2019.

Sigman, D. M., Altabet, M. A., McCorkle, D. C., Francois, R., and Fischer, G.: The $\delta^{15}N$ of nitrate in the southern ocean: Consumption of nitrate in surface waters, Global Biogeochem. Cycles, 13, 1149–1166, https://doi.org/10.1029/1999GB900038, 1999.

Sigman, D. M., Casciotti, K. L., Andreani, M., Barford, C., Galanter, M., and Böhlke, J. K.: A Bacterial Method for the Nitrogen Isotopic Analysis of Nitrate in Seawater and Freshwater, Anal. Chem., 73, 4145–4153, https://doi.org/10.1021/ac010088e, 2001.

Smart, S. M., Fawcett, S. E., Thomalla, S. J., Weigand, M. A., Reason, C. J. C., and Sigman, D. M.: Isotopic evidence for nitrification in the Antarctic winter mixed layer, Global Biogeochemical Cycles, 29, 427–445, https://doi.org/10.1002/2014GB005013, 2015.

Smith, W. O. and Nelson, D. M.: Importance of Ice Edge Phytoplankton Production in the Southern Ocean, BioScience, 36, 251–257, https://doi.org/10.2307/1310215, 1986.

Soppa, M., Völker, C., and Bracher, A.: Diatom Phenology in the Southern Ocean: Mean Patterns, Trends and the Role of Climate Oscillations, Remote Sensing, 8, 420, https://doi.org/10.3390/rs8050420, 2016.

Spira, T., Swart, S., Giddy, I., and du Plessis, M.: The Observed Spatiotemporal Variability of Antarctic Winter Water, Journal of Geophysical Research: Oceans, 129, e2024JC021017, https://doi.org/10.1029/2024JC021017, 2024.

Studer, A. S., Sigman, D. M., Martínez-García, A., Benz, V., Winckler, G., Kuhn, G., Esper, O., Lamy, F., Jaccard, S. L., Wacker, L., Oleynik, S., Gersonde, R., and Haug, G. H.: Antarctic Zone nutrient conditions during the last two glacial cycles: ANTARCTIC ZONE NUTRIENT CONDITIONS, Paleoceanography, 30, 845–862, https://doi.org/10.1002/2014PA002745, 2015.

Taylor, M. H., Losch, M., and Bracher, A.: On the drivers of phytoplankton blooms in the Antarctic marginal ice zone: A modeling approach, Journal of Geophysical Research: Oceans, 118, 63–75, https://doi.org/10.1029/2012JC008418, 2013.

Thomas, R. K., Fawcett, S. E., Forrer, H. J., Robinson, C. M., and Knapp, A. N.: Estimates of the Isotope Effect for Nitrate Assimilation in the Indian Sector of the Southern Ocean, Journal of Geophysical Research: Oceans, 129, e2023JC020830, https://doi.org/10.1029/2023JC020830, 2024.

Thompson, A. F., Heywood, K. J., Thorpe, S. E., Renner, A. H. H., and Trasviña, A.: Surface Circulation at the Tip of the Antarctic Peninsula from Drifters, Journal of Physical Oceanography, 39, 3–26, https://doi.org/10.1175/2008JPO3995.1, 2009.

Uotila, P., Holland, P. R., Vihma, T., Marsland, S. J., and Kimura, N.: Is realistic Antarctic sea-ice extent in climate models the result of excessive ice drift?, Ocean Modelling, 79, 33–42, https://doi.org/10.1016/j.ocemod.2014.04.004, 2014.

Vernet, M., Martinson, D., Iannuzzi, R., Stammerjohn, S., Kozlowski, W., Sines, K., Smith, R., and Garibotti, I.: Primary production within the sea-ice zone west of the Antarctic Peninsula: I—Sea ice, summer mixed layer, and irradiance, Deep Sea Research Part II: Topical Studies in Oceanography, 55, 2068–2085, https://doi.org/10.1016/j.dsr2.2008.05.021, 2008.

Vorrath, M.-E., Müller, J., Rebolledo, L., Cárdenas, P., Shi, X., Esper, O., Opel, T., Geibert, W., Muñoz, P., Haas, C., Kuhn, G., Lange, C. B., Lohmann, G., and Mollenhauer, G.: Sea ice dynamics in the Bransfield Strait, Antarctic Peninsula, during the past 240 years: a multi-proxy intercomparison study, Climate of the Past, 16, 2459–2483, https://doi.org/10.5194/cp-16-2459-2020, 2020.

Wang, W. L., Fu, W., Le Moigne, F. A. C., Letscher, R. T., Liu, Y., Tang, J. M., and Primeau, F. W.: Biological carbon pump estimate based on multidecadal hydrographic data, Nature, 624, 579–585, doi:10.1038/s41586-023-06772-4, 2023.

Wang, X. and Wu, Z.: Variability in Polar Sea Ice (1989–2018), IEEE Geosci. Remote Sensing Lett., 18, 1520–1524, https://doi.org/10.1109/LGRS.2020.3004257, 2021.

Wanninkhof, R., Johnson, K., Williams, N., Sarmiento, J., Riser, S., Briggs, E., Bushinsky, S., Carter, B., Dickson, A., Feely, R., Gray, A., Juranek, L., Key, R., Talley, L., Russel, J., and Verdy, A.: An Evaluation of pH and NO_3 Sensor Data from SOCCOM Floats and their Utilization to Develop Ocean Inorganic Carbon Products, Marine Science Faculty Publications, 1342, 30 pp., https://digitalcommons.usf.edu/msc_facpub/1342/, 2016. [Accessed: April 2024]

1101 Waser, N., Yin, K., Yu, Z., Tada, K., Harrison, P., Turpin, D., and Calvert, S.: Nitrogen isotope fractionation during
1102 nitrate, ammonium and urea uptake by marine diatoms and coccolithophores under various conditions of N availability,
1103 Mar. Ecol. Prog. Ser., 169, 29–41, https://doi.org/10.3354/meps169029, 1998.

1104 Weigand, M. A., Foriel, J., Barnett, B., Oleynik, S., and Sigman, D. M.: Updates to instrumentation and protocols for
1105 isotopic analysis of nitrate by the denitrifier method, Rapid Commun. Mass Spectrom., 30, 1365–1383,
1106 https://doi.org/10.1002/rcm.7570, 2016.

1107 Williams, G., Maksym, T., Wilkinson, J., Kunz, C., Murphy, C., Kimball, P., and Singh, H.: Thick and deformed
1108 Antarctic sea ice mapped with autonomous underwater vehicles, Nature Geosci, 8, 61–67,
1109 https://doi.org/10.1038/ngeo2299, 2015.

1110 Yoshikawa, C., Yamanaka, Y., and Nakatsuka, T.: An Ecosystem Model Including Nitrogen Isotopes: Perspectives
1111 on a Study of the Marine Nitrogen Cycle, J Oceanogr, 61, 921–942, https://doi.org/10.1007/s10872-006-0010-5, 2005.

1112 Yoshikawa, C., Ogawa, N. O., Chikaraishi, Y., Makabe, A., Matsui, Y., Sasai, Y., Wakita, M., Honda, M. C., Mino,
1113 Y., Aita, M. N., Fujiki, T., Nunoura, T., Harada, N., and Ohkouchi, N.: Nitrogen Isotopes of Sinking Particles Reveal
1114 the Seasonal Transition of the Nitrogen Source for Phytoplankton, Geophysical Research Letters, 49, e2022GL098670,
1115 https://doi.org/10.1029/2022GL098670, 2022.

1116 Yoshikawa, C., Shigemitsu, M., Yamamoto, A., Oka, A., and Ohkouchi, N.: A nitrogen isoscape of phytoplankton in
1117 the western North Pacific created with a marine nitrogen isotope model, Front. Mar. Sci., 11, 1294608,
1118 https://doi.org/10.3389/fmars.2024.1294608, 2024.

1119 Zehr, J. P. and Capone, D. G.: Biogeography of N2 Fixation in the Surface Ocean, in: Marine Nitrogen Fixation,
1120 edited by: Zehr, J. P. and Capone, D. G., Springer International Publishing, Cham, 117–141,
1121 https://doi.org/10.1007/978-3-030-67746-6_7, 2021.

1122 Zhou, X., Zhu, G., and Hu, S.: Influence of tides on mass transport in the Bransfield Strait and the adjacent areas,
1123 Antarctic, Polar Science, 23, 100506, https://doi.org/10.1016/j.polar.2020.100506, 2020.

1124

1125

1126